The role of mitochondria in autoimmune plasmablasts generation in lupus

Sung Hoon Jang

Department of Medical Science

The Graduate School, Yonsei University

The role of mitochondria in autoimmune plasmablasts generation in lupus.

Directed by Professor Jungsik Song

The Master's Thesis
submitted to the Department of Medical Science,
the Graduate School of Yonsei University
in partial fulfillment of the requirements for the degree of
Master of Medical Science

Sung Hoon Jang

December 2023

December 2023

This certifies that the Master's Thesis of
Sung Hoon Jang is approved.

Thesis Supervisor : Kihyuck Kwak

Thesis Committee Member#1 : Jungsik Song

Thesis Committee Member#2 : Ho-Keun Kwon

The Graduate School
Yonsei University

ACKNOWLEDGEMENTS

I sincerely express my gratitude to Professor Jungsik Song of Yonsei University, my mentor during my master's degree, who gave me invaluable guidance and teachings for research during my degree. Also, I sincerely thank Professor Kihyuck Kwak and Professor Ho-Keun Kwon for taking charge of the jury and giving important advice to complete the master's degree.

Despite encountering various challenges, I was able to finish my degree thanks to the assistance and support of many individuals around me. I extend my appreciation to all of them for all their support and consideration. I wish to express my gratitude to Ji-eun Kim, Joo Sung Shim, and Eun Gyeol Shin for their invaluable support during my time in the laboratory.

It was a blessing from God for me to be able to research with the individuals mentioned.

<TABLE OF CONTENTS>

LIST OF FIGURES

LIST OF TABLES

ABSTRACT

The role of mitochondria in autoimmune plasmablasts generation in lupus.

Sung Hoon Jang

Department of Medical Science
The Graduate School, Yonsei University

(Directed by Professor Jungsik Song)

Lupus is an autoimmune disease characterized by autoantibody production against nuclear antigens. Recent studies have revealed that extrafollicular (EF) B cells, which can differentiate into plasmablasts, play an important role in lupus. We investigated the role of mitochondrial oxidative phosphorylation (OXPHOS), glutamine metabolism, and CXCR4 expression in autoreactive plasmablasts generation.

For *in vivo* experiments, mice were stimulated with CpG-oligodeoxyribonucleotides (ODN) for 10 days to induce the differentiation of autoreactive plasmablasts. Immune cell subtypes and their mitochondrial mass and activity were measured by flow cytometry using spleen, blood, and bone marrow samples. The generation of autoreactive plasmablasts was evaluated by measuring serum anti-dsDNA antibodies and anti-dsDNA antibody-secreting cells. For the *in vitro* experiments, mouse splenocytes and peripheral blood mononuclear cells (PBMCs) from patients with lupus were stimulated with ODN for three days, and the generation of EF B cells was examined by flow cytometry. An OXPHOS inhibitor (IM156), glutamine metabolism inhibitor (CB-839), and CXCR4 inhibitor (AMD3100) were used.

In vivo ODN injection increased the proportion of B cell differentiation into plasmablasts with higher mitochondrial activity and CXCR4 expression. The ODN injection induced anti-dsDNA antibody-specific plasmablasts as well as increased the levels of anti-dsDNA antibodies. *In vitro* ODN treatment induced EF B cells from mouse splenocytes and

human PBMCs, which are dependent on mitochondrial metabolism. A combination strategy with IM156 and CB-839 or AMD3100 synergistically suppressed autoreactive plasmablasts.

This study demonstrated that mitochondrial metabolism, glutamine metabolism, and CXCR4-CXCL12 axis have a central role in the development of autoreactive plasmablasts, while the combination of IM156 and CB-839 or AMD3100 suppressed autoreactive plasmablasts by inhibiting mitochondrial OXPHOS, glutamine metabolism, and CXCR4-CXCL12 axis. The combination strategy could be a promising candidate for the treatment of autoimmune diseases characterized by aberrant B cell mitochondrial metabolism and CXCR4 expression.

Key words : mitochondria, glutamine, CXCR4, plasmablast, lupus

The role of mitochondria in autoimmune plasmablasts generation in lupus.

Sung Hoon Jang

Department of Medical Science
The Graduate School, Yonsei University

(Directed by Professor Jungsik Song)

I. INTRODUCTION

Systemic lupus erythematosus(SLE) is a chronic autoimmune disease characterized by the presence of autoantibodies against nuclear antigens, such as DNA, RNA, and histones (1, 2). It has been known that dysregulated signals downstream of the B cell receptors and toll-like receptors can initiate breaks in B cell tolerance to autoantigens (3). Furthermore, extrafollicular (EF) B cells are critical for the development of autoantibodies in lupus (4). The EF B cells can differentiate into plasmablasts, which produce class-switched low-affinity antibodies (5). Therefore, it is important to understand the metabolic pathways in autoreactive plasmablast generation in SLE.

Toll-like receptor 9 (TLR9) recognizes unmethylated CpG motifs in bacterial and viral DNA and is essential for the initiation of immune responses against pathogens (6). Interestingly, TLR9 signaling pathways are involved in the EF B cell activation and also in the process of autoantibody production in lupus (7, 8). Mitochondria are highly dynamic organelles with key functions in cellular activities, such as ATP production, calcium signaling, reactive oxygen species generation, and apoptosis (9). The B cells rely on mitochondrial metabolism to promote energy-intensive processes, including antibody production, cell proliferation, and differentiation to plasmablasts (10).

We have previously shown that suppression of OXPHOS metabolism by the complex I inhibitor IM156 downregulates autoantibody production and improves survival in a mouse model of lupus (9). Furthermore, recent evidence in the literature indicates that

glutamine metabolism is closely related to B cell activation and differentiation (11, 12, 13). Of note, CB-839 is an inhibitor of glutaminase-1 (GLS1), which plays a critical role in glutamine metabolism in B cells (11).

Interestingly, the complex I inhibitor, metformin, reportedly increases the dependency on glutamine metabolism while glutaminase inhibitors increase sensitivity to metformin in cancer (14). It is therefore plausible that OXPHOS inhibition may upregulate glutaminolysis to generate TCA (tricarboxylic acid) cycle intermediates. As such, combination therapy of OXPHOS and glutamine metabolism inhibition has been investigated in cancer and presents a promising way to reprogram cancer metabolism (15, 16). However, the interplay between OXPHOS and glutamine metabolism has not been sufficiently investigated in the context of autoimmune diseases.

CXCR4 and its ligand CXCL12 (also known as stromal cell-derived factor 1 or SDF-1) play important roles in many physiological processes, including embryogenesis, immune system regulation, and cancer progression (17). CXCR4 is a G protein-conjugated receptor expressed on the surface of various cell types, including hematopoietic stem cells, progenitor cells, immune cells, and cancer cells (18). CXCL12 is produced by stromal cells, and its expression is regulated by various stimuli, including hypoxia and inflammation (19). The chemokine receptor CXCR4 is expressed in various developmental stages of B cells (20). In particular, the expression of CXCR4 is highest in antibody-secreting cells (ASC), and the expressed CXCR4 moves ASC to the bone marrow (21).

IM156 downregulates autoantibody production and improves survival in a mouse model of lupus (22). Furthermore, recent evidence in the literature indicates that glutamine metabolism is closely related to B cell activation and differentiation (11, 12, 13). AMD3100, also known as Plerixafor, is a small molecule inhibitor of CXCR4. AMD3100 binds to the extracellular domain of CXCR4 and blocks the binding of CXCL12, thereby inhibiting CXCR4 signaling and downstream cellular responses (23).

In this study, we aimed to assess the efficacy of a combination strategy of IM156 with

CB-839 or AMD3100 to suppress autoreactive plasmablasts.

II. MATERIALS AND METHODS

1. *In vitro* mouse B cell experiments

Mouse splenic and bone marrow cells were stimulated with 1 μM ODN (Class B CpG-oligodeoxyribonucleotides1826; Bioneer, Daejeon, Korea) and 25 ng/ml IL-21 (PeproTech, Cranbury, NJ, USA) for three days. The cells were also treated with IM156 (ImmunoMet Therapeutics, Houston, TX, USA) All stimulants and chemicals were diluted in RPMI-1640 (Hyclone, Logan, UT, USA) with FBS (Cytiva, Marlborough, MA, USA) and penicillin-streptomycin (Hyclone).

2. *In vivo* B cell activation by CpG-ODN

An ODN-injected mouse model was established following the methods described in a previous study (24, 25). Seven-week-old B6 mice (C57BL/6; Orient Bio, Seoul, Korea) were injected intraperitoneally with 50 μg of ODN1826 on days 1, 3, 5, 7, and 9. Mice in the IM156, CB-839, and AMD3100 treatment groups were intraperitoneally injected with IM156, CB-839, and/or AMD3100 as indicated on days 0, 2, 4, 6, and 8. On day 10, the mice were euthanized, and spleen, bone marrow, and blood samples were collected for further analysis.

3. *In vitro* human B cell experiments

Human whole blood was collected after obtaining written informed consent from patients with SLE and approval by the Severance Hospital IRB program (4-2020-0996). Peripheral blood mononuclear cells (PBMCs) were isolated by Ficoll-Paque™ PLUS (GE Healthcare, Chicago, IL, USA). Isolated PBMCs were stimulated with 1 μM ODN (Class B CpG-ODN 2006; Bioneer) and 25 ng/ml IL-21 for three days. The PBMCs were also treated with IM156.

4. Flow cytometry

The cells were stained for 20 min at 37 °C with the antibodies and chemicals listed in

Table 1. For the measurement of mitochondrial mass and activity, MitoTracker Deep Red (MTDR) and MitoTracker Green (MTG) were used (26). For the measurement of fatty acid uptake, we utilized BODIPY. For the measurement of glucose uptake, we utilized 2-[N-(7-nitrobenz-2-oxa-1,3-diazol-4-yl) amino]-2-deoxy-D-glucose (2-NBDG). Data acquisition was performed using a BD LSRFortessa™ Cell Analyzer (BD Biosciences, Franklin Lakes, NJ, USA), and data were analyzed using FlowJo, version 10 (Tree Star, Ashland, OR, USA).

5. Enzyme-linked immunosorbent assay

Serum anti-double strand DNA IgG concentrations in mice were measured by enzyme-linked immunosorbent assay (ELISA). Venous blood was collected from mice retro-orbitally and centrifuged for 10 min at 1000 × g. A 96-well Microtest assay plate (Corning, New York, NY, USA) was coated with 100 μg/ml dsDNA (Sigma-Aldrich, St. Louis, MO, USA) and blocked with 5% FBS and 3% BSA in PBS. Next, diluted serum samples (1:100) were loaded, and the diluted (1:4000) anti-mouse IgG-horseradish peroxidase (Cell Signaling, Danvers, MA, USA) was added. The bound enzymes were developed by adding TMB solution (Invitrogen, Carlsbad, CA, USA), and the reaction was stopped by adding 1 M H_2SO_4. The plates were read at 450 nm.

6. Enzyme-linked immunospot assay

The number of anti-dsDNA IgG-secreting cells was measured by an enzyme-linked immunospot assay (ELISPOT) on murine splenic and bone marrow cells used as samples. A PVDF-96-well MultiScreen plate (Millipore, Burlington, MA, USA) was activated with 35% ethanol for 30 s. The plate was next coated with 100 μg/ml dsDNA and blocked with 5% FBS and 3% BSA in PBS. Mouse splenic and bone marrow cell samples were loaded, and a diluted (1:10000) anti-mouse IgG-HRP was added. The bound enzymes were developed by adding a TMB solution. The plates were observed using a CTL ImmunoSpot S6 Micro Analyzer (ImmunoSpot, Shaker Heights, OH, USA).

7. Mouse splenic B cell and human PBMC transcriptome analysis

RNA sequencing (RNA-seq) data from our previous study were reanalyzed to evaluate activated metabolic pathways during B cell differentiation with ODN. In brief, mouse spleen B cells were isolated using magnetically activated cell sorting on day 4 after ODN injection with or without IM156 treatment, and RNA sequencing was performed. Gene set enrichment analysis (GSEA) was used to assess transcript expression changes in metabolic pathways from GO Biological Process gene sets and Reactome gene sets. To evaluate activated metabolic pathways in lupus, human RNA-seq data from a publicly available SLE transcriptome study was used (27). In brief, RNA-seq data from whole blood of 79 patients with active SLE, 46 inactive SLE patients, and age/sex-matched 58 healthy donors were analyzed with the same GSEA used for mouse B cell transcriptome analysis.

8. Chemotaxis assay

Transmigration of mouse B cells and Human B cells by CXCR4 was assessed in 6.5mm diameter 24 Transwell chemotaxis chambers (35224, SPL, South Korea) with a pore size of 8 μm. The mouse splenic cells were stimulated with 1 μM ODN(Class B CpG-ODN 1826, Bioneer, Daejeon, Korea) and 25ng/ml IL-21(210-21, PeproTech, USA). IM156(ImmunoMet Therapeutics, Houston, TX, USA) and AMD3100 (35569, Cayman chemical, USA) were treated to stimulated mouse splenic as indicated. All stimulants and chemicals were diluted in RPMI-1640(SH30255.01, Hyclone, USA) with FBS(SH30919.03, cytiva, USA) and s.p. (SV30010, Hyclone, USA). 1×10^6 cells were loaded in upper chamber, 100ng of SDF-1 (250-20A, PeproTech, USA) in 600μl RPMI-1640(SH30255.01, Hyclone, USA) was loaded well. The chambers were incubated for 4h at 37°C in 5% CO2. After incubation, cells that migrated into the wells were counted and analyzed using flow cytometry

9. *In vitro* Th17 cell differentiation

Mouse T cells were isolated from spleens using a CD4+ T cell isolation kit (Stemcell technology, Vancouver, Canada). Cells were cultured in IMDM (Welgene, Gyeongsan, Korea) supplemented with 10% heat-inactivated FBS (Hyclone), 10U/ml penicillin-streptomycin (Welgene), 10 mg/ml gentamicin (Welgene), 4 mM L-glutamine, and 50 mM b-mercaptoethanol (Gibco, Waltham, MA, USA). For T cell polarization, 1 x 10^5 cells were seeded in 96-well plates that were pre-coated with a 1:20 dilution of goat anti-hamster IgG in PBS. Naive T cells were primed with anti-CD3ε (0.25 mg/mL) and anti-CD28 (1 mg/mL) for 24 hours prior to polarization. Cells were further cultured for 48h under Th17-lineage polarizing condition; 0.3 ng/mL TGF-β, 20 ng/mL IL-6, 20ng/mL IL-23, 2.5 mg/mL anti-IL-4, 2.5 mg/mL anti-IFNγ. Cells were also treated with IM156 (ImmunoMet Therapeutics, Houston, TX, USA) and CB-839 (TargetMol, Boston, MA, USA).

10. Extracellular flux analysis

Real-time analysis of the oxygen consumption rate (OCR) was conducted using the Seahorse XF24 extracellular flux analyzer (Agilent, Santa Clara, CA, USA). The Daudi cell line was seeded at a density of 5×10^5 cells/well in XF24 plates (Agilent). The plated cells were cultured in Seahorse XF RPMI Medium (Agilent) under growth conditions for 24 hours. Subsequently, the cells were pretreated with or without varying concentrations of IM156 and/or CB-839 for 24 hours. The perturbation profile was measured in accordance with the manufacturer's instructions.

11. Statistical analyses

P-values were calculated using a two-tailed Student's t-test and one-way ANOVA, with a post hoc Tukey's multiple comparison test (GraphPad version 9).

12. Study approval

All experimental procedures and daily care were conducted in accordance with the IACUC guidelines of the Yonsei University Health System (2021-0231). All mice were maintained under specific pathogen-free conditions at a controlled temperature (23 ± 3 °C) and relative humidity (40–60%).

Table 1. List of antibodies and chemicals used for flow cytometry

Antibodies/chemicals	**Source**	**Identifier**
Pacific Blue anti-mouse CD19	BioLegend	#115523
Alexa Fluor 700 anti-mouse CD11c	BioLegend	#117320
PE/Cyanine7 anti-mouse/human CD11b	BioLegend	#101216
APC anti-mouse CD19	BioLegend	#152410
APC/Cyanine7 anti-mouse CD38	BioLegend	#102728
PE/Cyanine7 anti-mouse CD138	BioLegend	#142514
FITC anti-mouse/human CD11b	BD Biosciences	#553310
Alexa Flour 700 anti-mouse CD4	BD Biosciences	#557956
PE anti-mouse CD23	BioLegend	#101607
PE/Cy7 anti-mouse CD21/CD35	BioLegend	#123419
Brillant Violet 605 anti-mouse CD95	BioLegend	#152612
PE, Anti-Mo IL-21	eBioscience	#12-7211-80
eFluor 450 anti-mouse IL-17A	eBioscience	#48-7177-82
PE Mouse anti-Mouse RORγt	BD Biosciences	#562607
FITC anti-human CD19	BD Biosciences	#560994
APC/Cyanine7 anti-human CD11c	BioLegend	#337217
PE anti-mouse CD184 (CXCR4) Antibody	BioLegend	#146506
MitoTracker Deep Red (MTDR)	Invitrogen	#M22426
MitoTracker Green (MTG)	Invitrogen	#M7514
JC-1	Invitrogen	#T3168
2-NBDG	Invitrogen	#N13195

BODIPY	Invitrogen	#D3922
7-AAD	Invitrogen	#A1310

III. RESULTS

1. CpG-ODN induces autoreactive EF B cells and plasmablasts

To investigate the generation of autoreactive EF B cells and plasmablasts, we injected mice with 50 μg of ODN1826 intraperitoneally every other day for 10 days and measured the EF B cells (CD19+, CD11c+, and CD11b+ cells) to CD19 ratio in the mouse spleen and the plasmablast (CD19+, CD38+, and CD138+ cells) to CD19 B cells ratio in the mouse PBMCs, and bone marrow. EF B cells and plasmablasts gradually increased over time from day 0 to day 4 and day 10 (Figure 1A, B, C, D, E, F). All of the plasmablasts generated by ODN injection expressed CD11c and CD11b, which are EF B cell markers. (Figure 1G). In ODN injected mice EF B cell, not other B cell subsets, significantly increased (Figure 1H). These results indicate that EF B cells are the origin of plasmablasts in ODN-injected mice. To assess the autoreactive B cell differentiation, we performed anti-dsDNA IgG ELISA and anti-dsDNA IgG ELISPOT. Anti-dsDNA IgG was elevated in the serum of ODN-injected mice on day 10 (Figure 1I). anti-dsDNA IgG-secreting cells were detected in bone marrow samples from ODN-injected mice (Figure 1J, K). Together, our findings indicate that the TLR9 agonist induces the generation of EF B cells and the differentiation of EF B cells into autoreactive plasmablasts.

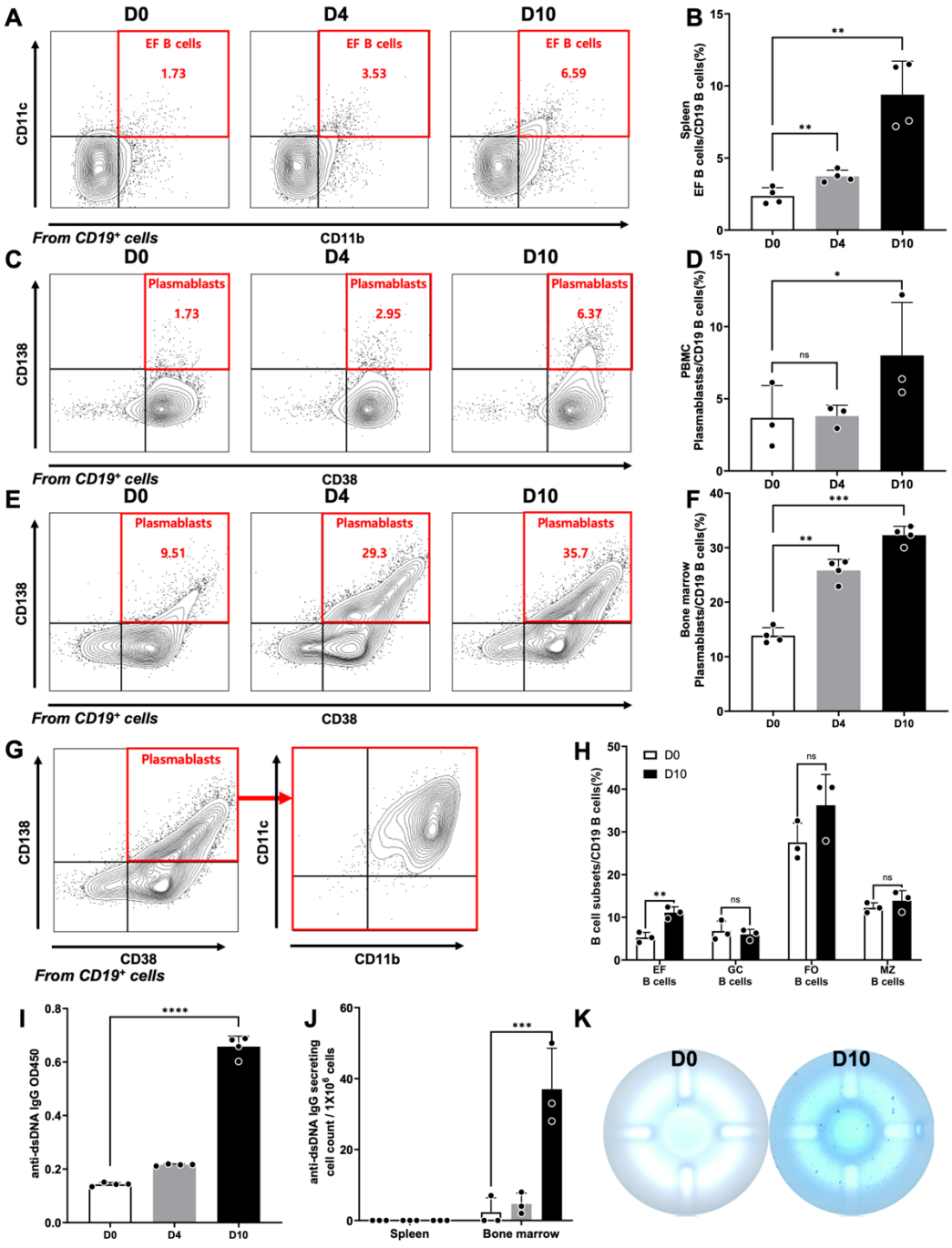

Figure 1. ODN induces autoreactive EF B cells and plasmablasts. (A) Flow cytometry

results of CD19+ CD11c+ CD11b+ EF B cells in the mouse spleen. **(B)** Percentage ratio of EF B cells in the mouse spleen. **(C)** Flow cytometry results of CD19+ CD38+ CD138+ plasmablasts in the mouse blood. **(D)** Percentage ratio of plasmablasts in the mouse blood. **(E)** Flow cytometry results of CD19+ CD38+ CD138+ plasmablasts in the mouse bone marrow. **(F)** Percentage ratio of plasmablasts in the mouse bone marrow. **(G)** Flow cytometric analysis of CD11c and CD11b in plasmablasts. **(H)** Percentage ratio of EF (extrafollicular) B cells (CD19+CD11b+CD11c+), GC (germinal center) B cells (CD19+CD38-Fas+), FO (follicular) B cells (CD19+CD23+CD21int), and MZ (marginal zone) B cells (CD19+CD23-CD21-). **(I)** Serum anti-dsDNA IgG levels. **(J)** Counts of anti-dsDNA IgG-secreting cells in the bone marrow. **(K)** ELISPOT results of mouse bone marrow cells. D0 refers to ODN 0 days; D4 refers to ODN 4 days; D10 refers to ODN 10 days. Statistical significance was determined by a two-tailed Student's t-test. (*P < 0.05, **P < 0.01, ***P < 0.005, ****P < 0.001, ns, not significant; n = 3-4).

2. CpG-ODN activates mitochondrial metabolism in autoreactive plasmablast

To investigate metabolic changes with plasmablasts generation by TLR9 stimulation, we measured MTDR, MTG, JC-1, 2-NBDG, and BODIPY fluorescence in bone marrow cells. *In vivo* ODN stimulation increased mitochondrial activity in B cells and plasmablasts, as assessed by MTDR and MTG levels (Figure 2A, B). The JC-1 aggregate/monomer ratio showed that MMP was elevated in B cells and plasmablasts obtained by *in vivo* TLR9 stimulation (Figure 2C). Fatty acid uptake was also increased in bone marrow B cells and plasmablasts following ODN stimulation, while glucose uptake was decreased (Figure 2D, E). Mitochondrial activity continued to increase as plasmablasts migrated from the spleen to the blood and then to the bone marrow, particularly with ODN stimulation (Figure 2F). Together, our findings indicate that the TLR9 agonist induces activation of mitochondrial metabolism of autoreactive plasmablasts.

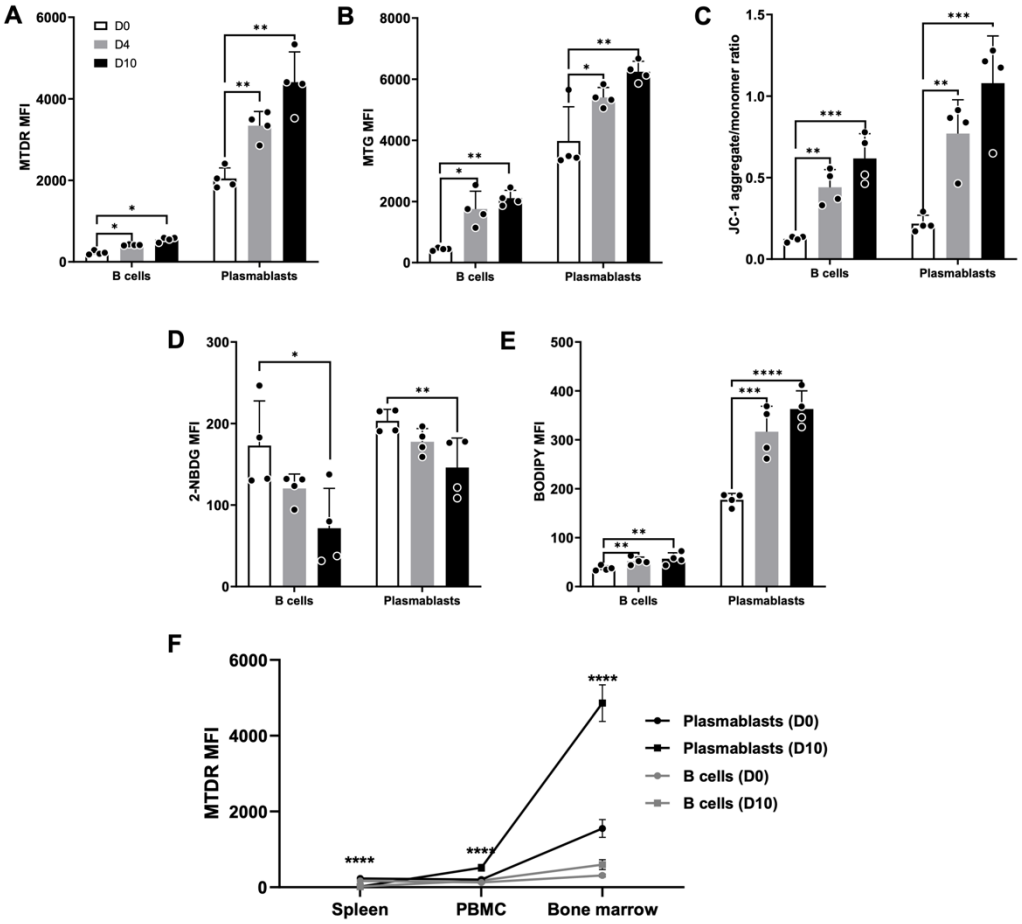

Figure 2. ODN induces mitochondrial activation in autoreactive plasmablasts. (A) Measurement of MitoTracker Deep Red (MTDR) in B cells and plasmablasts. **(B)** Measurement of MitoTracker Green (MTG) in B cells and plasmablasts. **(C)** Measurement of the mitochondrial membrane potential of B cells and plasmablasts using JC-1. **(D)** Measurement of glucose uptake of B cells and plasmablasts using 2-NBDG. **(E)** Measurement of fatty acid uptake of B cells and plasmablasts using BODIPY. **(F)** MTDR of B cells and plasmablasts in the spleen, PBMCs, and the bone marrow. Statistical significance was determined by a two-tailed Student's t-test (*P < 0.05, **P < 0.01, ***P < 0.005, ****P < 0.001; n = 4).

3. CpG-ODN induces mitochondrial metabolism pathway in autoreactive plasmablast

Next, we reanalyzed the RNA-Seq data from our previous study which was obtained using mouse splenic B cells on day 4 after ODN injection with or without IM156. To investigate key metabolic pathways of B cells activated through TLR9 signaling, we conducted a GSEA analysis on five essential metabolic pathways. We used three spleen samples from each experimental group to obtain RNA-seq data. Our GSEA results revealed significant alterations in pathways related to electron transport chain (ETC), fatty acid metabolism, and glutamine metabolism to ODN injection (ETC, $p = 0.010$; fatty acid metabolism, $p = 0.012$; glutamine metabolism, $p = 0.023$; Figure 3A, B). It is noteworthy that GSEA estimates the statistical significance of the normalized enrichment score (NES) through permutation tests. Because p-values from GSEA should be interpreted with caution, we also evaluated the false discovery rate (FDR) using q-values. Our analysis of FDR is consistent with p-values (ETC, $q = 0.101$; fatty acid metabolism, $q = 0.170$; glutamine metabolism, $q = 0.131$). More importantly, the findings of pathway enrichment analysis were consistent with the observed *in vivo* phenotype resulting from ODN injection, as assessed through measurements of MTDR, MTG, JC-1, 2-NBDG, and BODIFY (Figure 2A, B, C, D, E). The IM156 treatment in ODN-injected mice downregulated genes related to the ETC and the TCA cycle, but not glutamine metabolism (Figure 3C, D). ODN These results suggest that complex I inhibition by IM156 alone is not sufficient to reduce B cell mitochondrial metabolism induced by ODN.

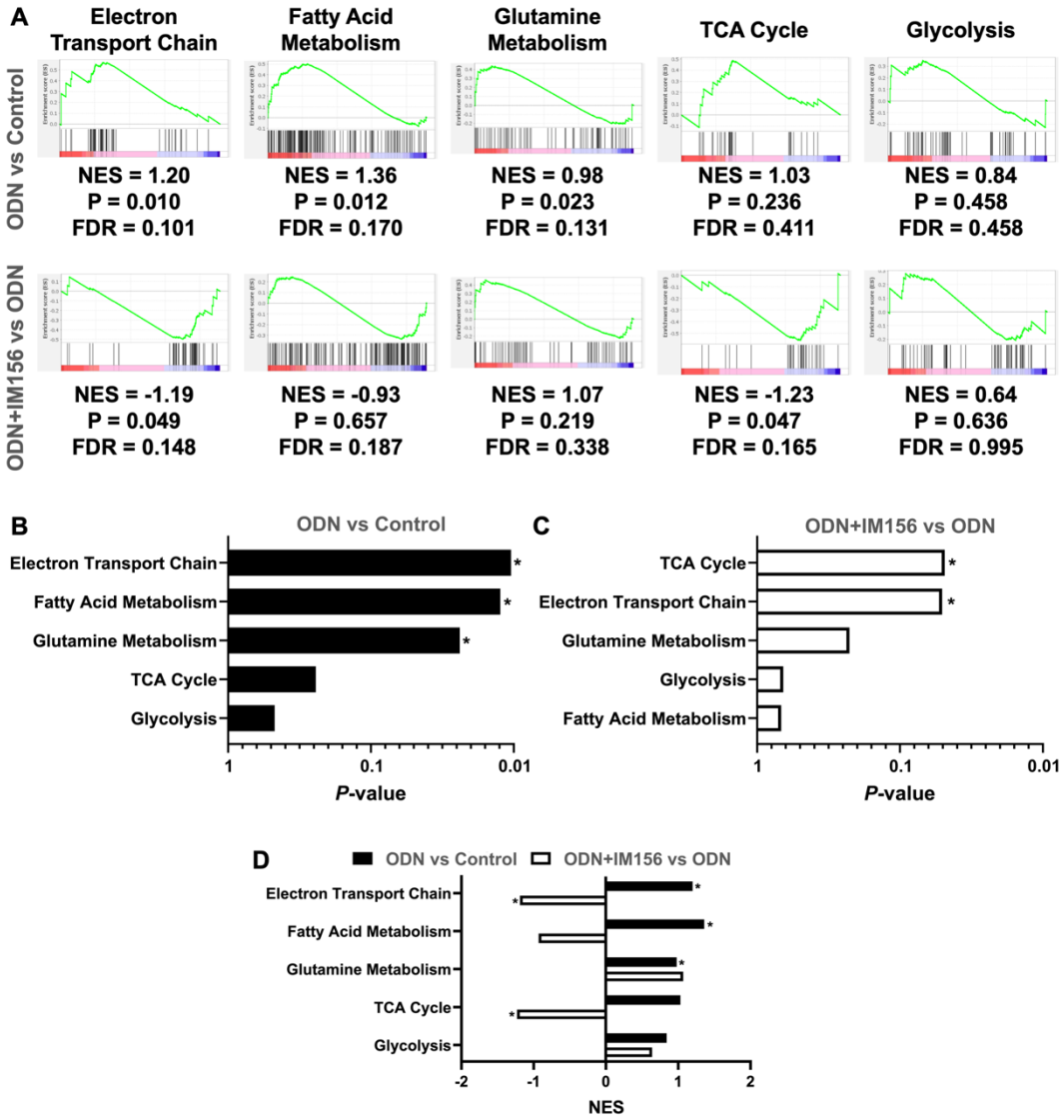

Figure 3. Transcriptome analysis of metabolic pathways in ODN-injected mouse splenic B cells with IM156. (A) Gene set enrichment analysis (GSEA) of the electron transport chain, fatty acid metabolism, glutamine metabolism, TCA cycle, and glycolysis. **(B)** P-values for comparisons between the control and ODN group in metabolism GSEA. A logarithmic scale is used on the X-axis. **(C)** P-values for comparisons between the ODN group and ODN+IM156 group in metabolism GSEA. A logarithmic scale is used on the

X-axis. **(D)** Normalized Enrichment Score (NES) for metabolism GSEA (*P < 0.05). A false discovery rate (FDR) of <0.25 between any two populations was considered significant; n = 3

4. The combination treatment of IM156 and CB-839 enhances the suppression of OCR

To evaluate the impact of IM156 and CB-839 on cellular respiration, we treated these inhibitors to Daudi B lymphoma cells individually and in combination. We assessed changes in OCR using the Seahorse XF24 extracellular flux analyzer. IM156 and CB-839 demonstrated a dose-dependent decrease in basal and maximal mitochondrial OCR (Figure 4A, B). Notably, the combination treatment with IM156 (5 μM) and CB-839 (5 μM) demonstrated a significant reduction in maximal mitochondrial OCR compared to IM156 or CB-839 alone (Figure 4C). Furthermore, the combination treatment with IM156 (5 μM) and CB-839 (5 μM) showed a significant reduction in both basal and maximal mitochondrial OCR compared to no treatment (Figure 4C, D).

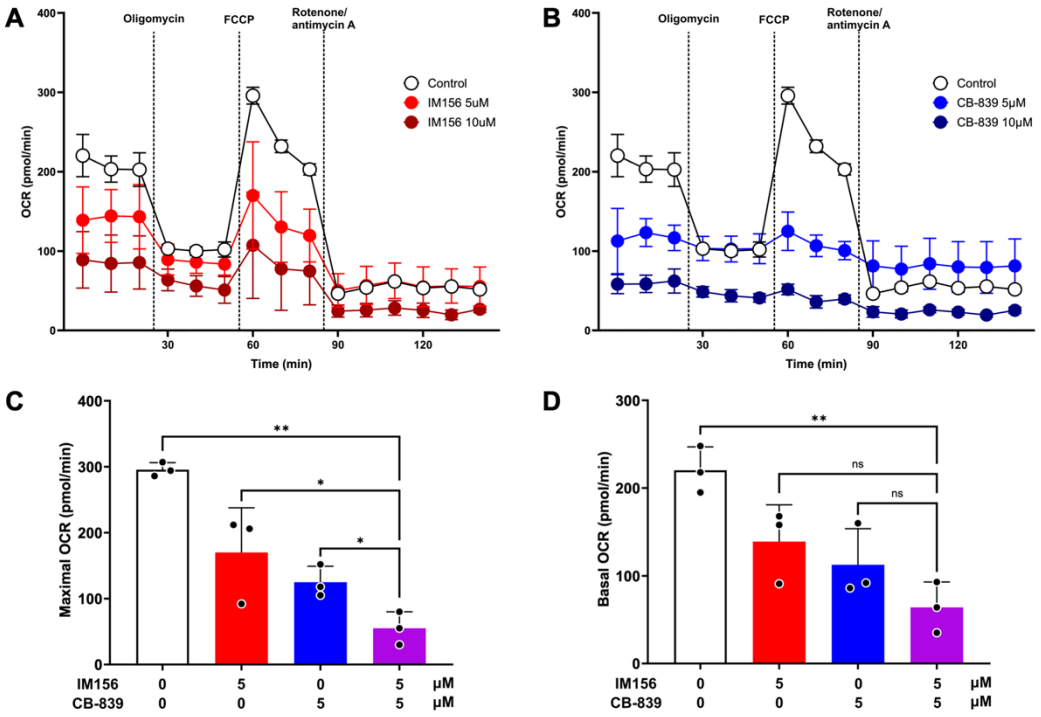

Figure 4. Extracellular flux analysis of Daudi B lymphoma cells with IM156, CB-839 alone and in combination. (**A**) Cellular oxygen consumption rates (OCR) of IM156 alone. (**B**) Cellular OCR of CB-839 alone. (**C**) OCR of maximal respiration with combination of IM156 and CB-839. (**D**) OCR of basal respiration with combination of IM156 and CB-839. Statistical significance was determined by two-tailed Student's t-test (*$P < 0.05$, **$P < 0.01$; n = 3).

5. IM156 suppresses mitochondrial metabolism of plasmablasts *in vivo*

Next, we evaluated the effect of IM156, an OXPHOS inhibitor, on EF B cells and plasmablast generation. IM156 significantly reduced EF B cells and plasmablasts. (Figure 5A, B, C). IM156 also significantly decreased mitochondrial activity (Figure 5D, E). anti-dsDNA antibody in mouse serum and anti-dsDNA IgG-secreting cells significantly reduced as the IM156 dose increased (Figure 5F, G). Collectively, these results demonstrate that selective suppression of mitochondrial metabolism by IM156 reduces autoantibody generation and improves the systemic inflammatory response.

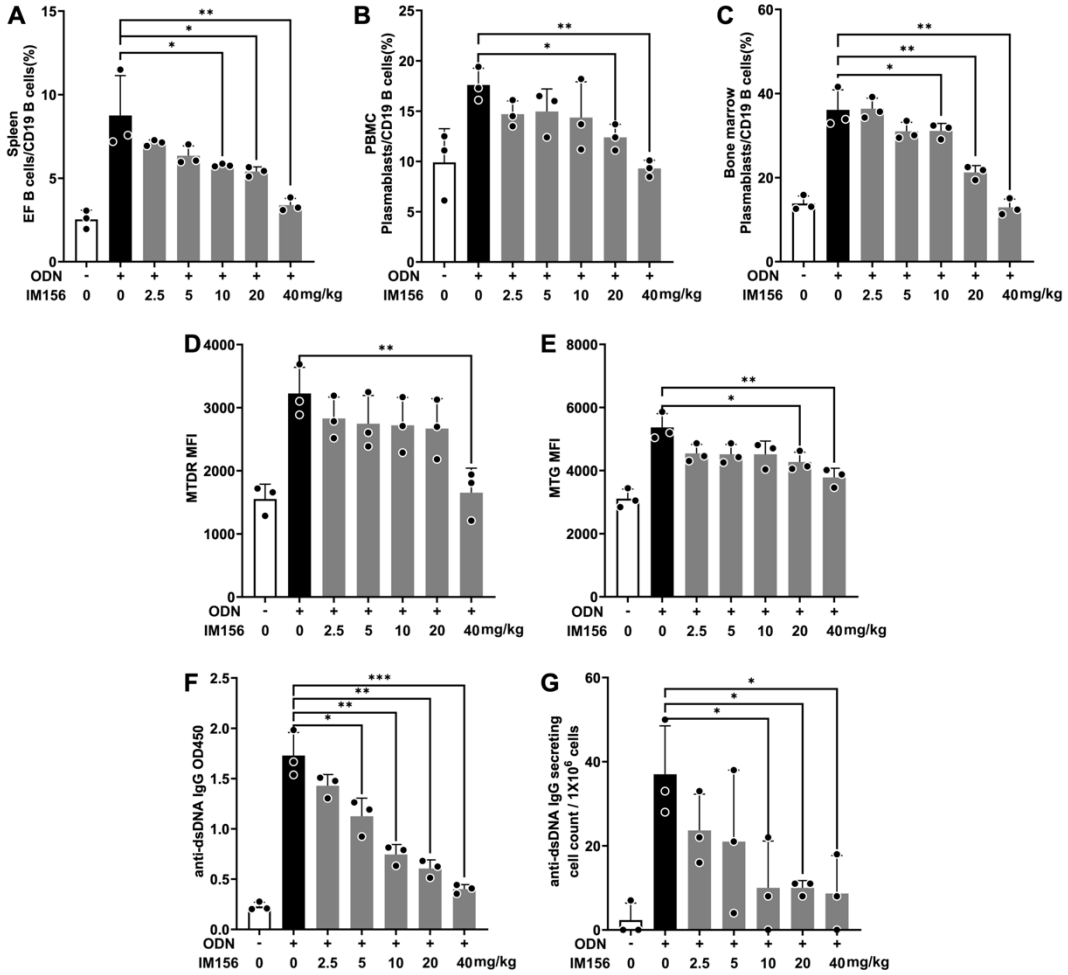

Figure 5. IM156 reduces autoreactive EF B cells and plasmablasts. (A) Percentage ratio of EF B cells in the mouse spleen with IM156. **(B)** Percentage ratio of plasmablasts in the mouse PBMCs with IM156. **(C)** Percentage ratio of plasmablasts in the mouse bone marrow with IM156. (**D)** Measurement of MitoTracker Deep Red (MTDR) in bone marrow plasmablasts with IM156. **(E)** Measurement of MitoTracker Green (MTG) in bone marrow plasmablasts with IM156. **(F)** Counts of anti-dsDNA IgG-secreting cells in the bone marrow with IM156. **(G)** Serum anti-dsDNA IgG levels with IM156. Statistical significance was determined by a two-tailed Student's t-test. (*P < 0.05, **P < 0.01, ***P < 0.005, ****P < 0.001; n = 3).

6. CB-839 suppresses mitochondrial metabolism of plasmablasts *in vivo*

Next, we evaluated the effect of CB-839, a glutamine metabolism inhibitor, on plasmablast generation. CB-839 significantly reduced MTDR in plasmablasts, while CB-839 alone did not change the plasmablasts/CD19 B cells ratio (Figure 6A, B). We also did not observe any significant changes in glucose and fatty acid uptake in response to CB-839 (Figure 6C, D). Although anti-dsDNA IgG titers in mouse serum decreased significantly by CB-839 (Figure 6E), the compound did not similarly affect the levels of anti-dsDNA IgG-secreting cells in the bone marrow (Figure 6F). Collectively, these results demonstrate that selective suppression of glutamine metabolism by CB-839 reduces autoantibody generation and improves the systemic inflammatory response.

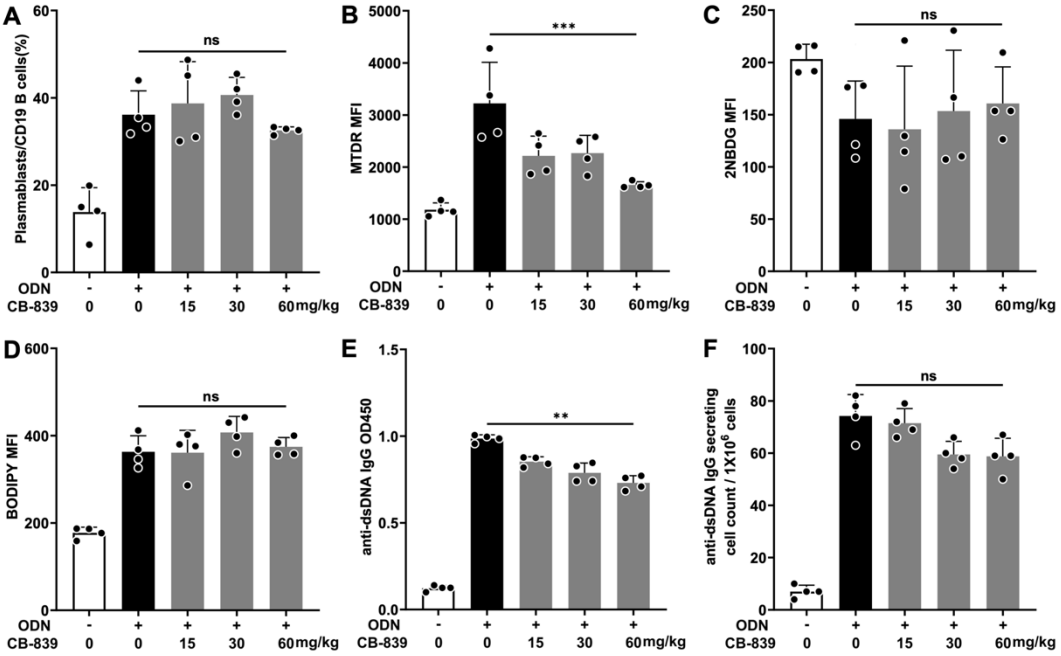

Figure 6. CB-839 downregulates autoantibody generation in ODN-injected mice by suppression of mitochondrial activity. (A) Percentage ratio of plasmablasts/CD19 B cells in the bone marrow. **(B)** Measurement of MTDR in bone marrow plasmablasts. **(C)** Glucose uptake measured by 2-NBDG. **(D)** Fatty acid uptake measured by BODIPY. **(E)** Serum anti-dsDNA IgG levels. **(F)** Counts of anti-dsDNA IgG-secreting cells in the bone marrow. Statistical significance was determined by one-way ANOVA (**P < 0.01, ***P < 0.005, ns, not significant; n = 4).

7. Combination strategy with IM156 and CB-839 reduces plasmablast generation *in vivo*

We examined the efficacy of the combination strategy using IM156 and CB-839 for the downregulation of autoreactive plasmablasts. IM156 decreased plasmablasts in mouse bone marrow, with CB-839 having a compounding effect (Figure 7A). Anti-dsDNA IgG-secreting cells, and anti-dsDNA IgG titers in mouse serum, were all decreased following treatment with IM156 and CB-839 (Figure 7B, C). In plasmablasts (CD19+CD38+CD138+), it is noteworthy that the markers associated with mitochondria metabolism, including MTDR and MTG fluorescence levels, as well as the JC-1 ratio, demonstrated no further reduction with the combination of IM156 and CB-839 as compared to IM156 monotherapy (Figure 7D, E, F). Conversely, in non-plasmablast B cells (CD19+CD38-CD138-), mitochondria metabolism markers were further reduced with the combination of IM156 and CB-839 as compared to IM156 monotherapy (Figure 7G, H, I). These results support that mitochondria metabolism plays a more important role for plasmablasts than for other B cell subsets. While the combination of IM156 and CB-839 synergistically suppressed the percentage of plasmablasts among CD19+B cells, the remaining plasmablasts maintained a similar level of mitochondrial metabolism. Taken together, these findings demonstrate that the combination of IM156 and CB-839 effectively reduces autoreactive plasmablast generation.

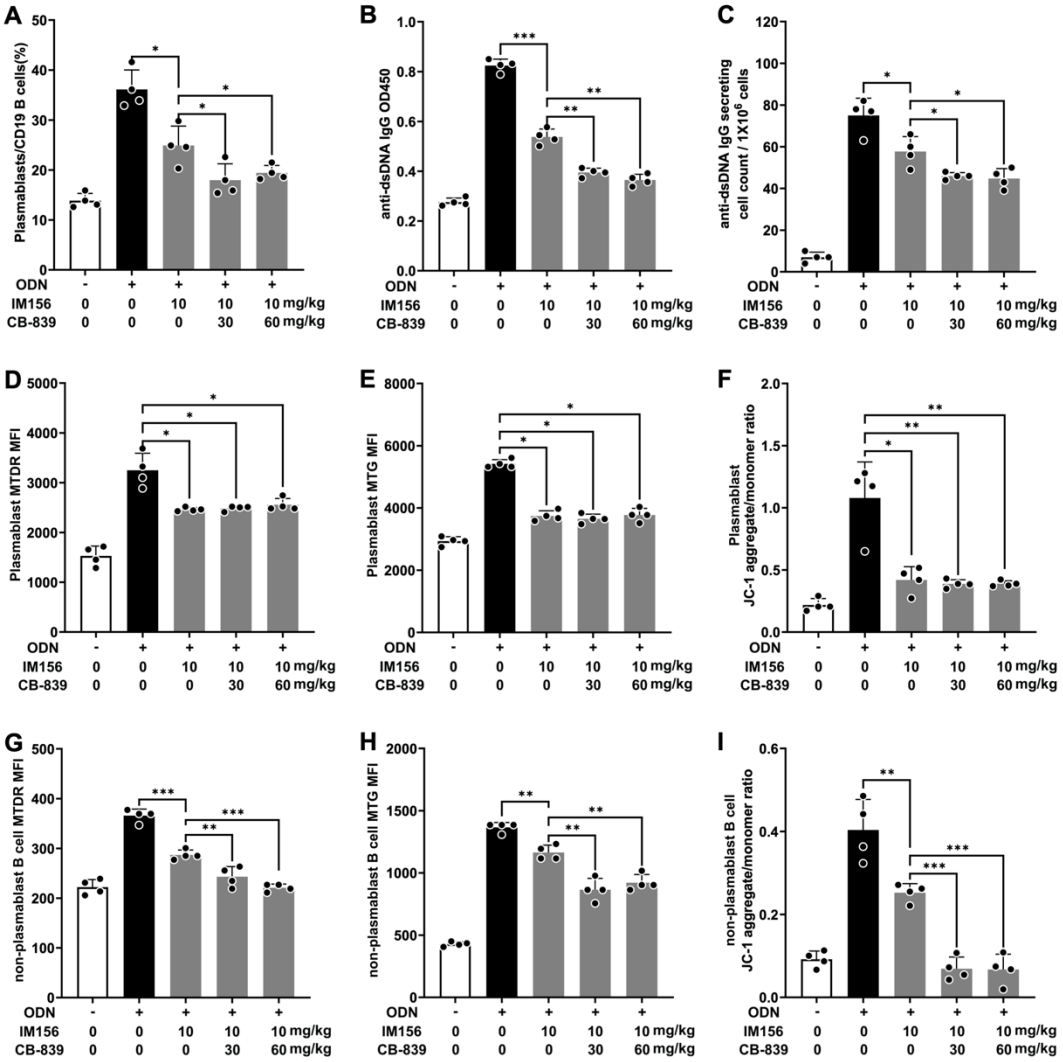

Figure 7. A combination therapy of IM156 and CB-839 downregulates autoreactive plasmablasts in ODN-injected mice. (A) Percentage ratio of plasmablasts/CD19 B cells in the bone marrow. **(B)** Serum anti-dsDNA IgG levels. **(C)** Counts of anti-dsDNA IgG-secreting cells in the bone marrow. Measurement of **(D)** MTDR, and **(E)** MTG, in bone marrow plasmablasts (CD19+CD38+CD138+). **(F)** Measurement of the MMP in bone marrow plasmablasts (CD19+CD38+CD138+) using JC-1. Measurement of **(G)** MTDR, **(H)** MTG, and **(I)** JC-1 aggregation/monomer ratio in bone marrow non-plasmablasts B

cells (CD19+CD38-CD138-). Statistical significance was determined by a two-tailed Student's t-test (*P < 0.05, **P < 0.01, ***P < 0.005, ****P < 0.001; n = 4).

8. Effect of IM156 and CB-839 on mouse plasma cells

We examined the selectivity of the IM156 and CB-839 combination strategy. Plasma cell (CD19-CD38+CD138+) generation was unaffected by ODN, IM156, or CB-839 (Figure 8A) while IM156 and CB-839 reduced mitochondrial mass and activity in these cells (Figure 8B).

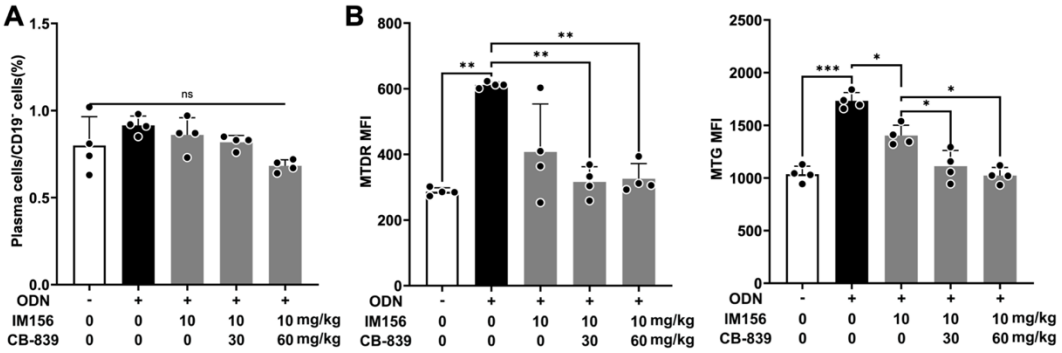

Figure 8. The effect of IM156 and CB-839 on plasma cells *in vivo*. (A) Percentage of plasma cells/CD19- cells in bone marrow following treatment with IM156 and CB-839. **(B)** Measurement of the mitochondrial activity and mass of bone marrow plasma cells using MitoTracker Deep Red (MTDR) and MitoTracker Green (MTG). Statistical significance was determined by two-tailed Student's t-test and one-way ANOVA. (*P < 0.05, **P < 0.01, ***P < 0.005, ns, not significant; n = 4).

9. Effect of OXPHOS inhibition on mouse EF B cells

Using mouse splenocytes, we investigated the effects of OXPHOS on the generation of EF B cells (CD11c+CD11b+CD19+). IM156 inhibits EF B cell generation by suppressing OXPHOS metabolism (Figure 9A, B).

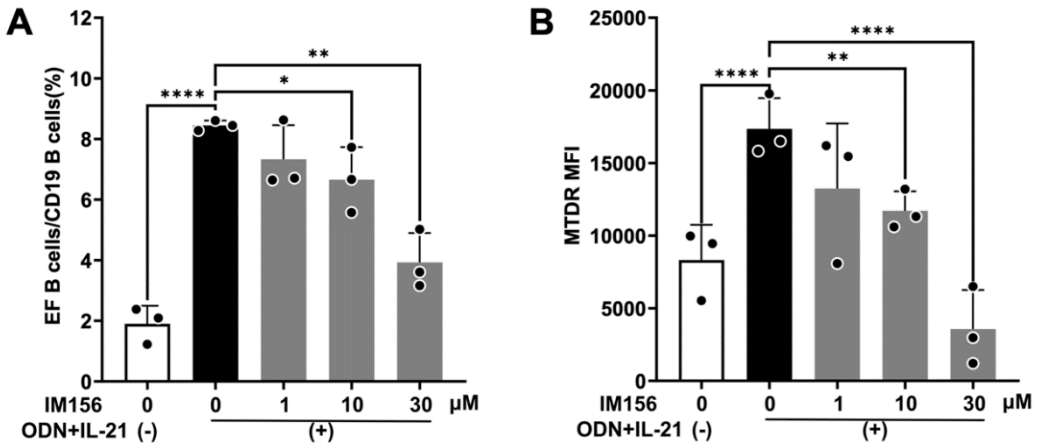

Figure 9. IM156 inhibits mouse splenic EF B cells in vitro differentiation. A concentration of ODN1826 1 μM and IL-21 25 ng/ml was used to induce in vitro mouse EF B cell differentiation. **(A)** Percentage ratio of EF B cells/CD19 B cells in splenocytes treated with IM156. **(B)** Measurement of MTDR in splenic EF B cells treated with IM156. Statistical significance was determined by two-tailed Student's t-test and one-way ANOVA. (*P < 0.05, **P < 0.01, ****P < 0.001; n = 3).

10. Effect of glutamine inhibition on mouse EF B cells

Using mouse splenocytes, we investigated the effects of glutamine metabolism on the generation of EF B cells (CD11c+CD11b+CD19+), the precursors of plasmablasts. We observed a positive correlation between glutamine concentration and the number of EF B cells (Figure 10A). The MTDR fluorescence levels in EF B cells also increased together with the concentration of glutamine (Figure 10B). We further investigated the effect of IM156 at different glutamine concentrations. IM156 more effectively attenuated the number and MTDR of EF B cells when glutamate was depleted from the growth medium compared to when glutamate was present (Figure 10C, D), suggesting a glutamate dependency upon OXPHOS inhibition. As the CB-839 concentration increased, the number and MTDR of EF B cells decreased (Figure 10E, F). The combination of CB-839 and IM156 had a compounding inhibitory effect on the number and MTDR of EF B cells (Figure 10G, H). In our *in vitro* study, we observed no alterations in cell viability at the dosages of IM156 and CB-839 employed (Figure 10I, J). These results suggest that IM156 increases glutamate dependency during ODN-induced B cell differentiation, while CB-839 synergistically downregulates EF B cell generation.

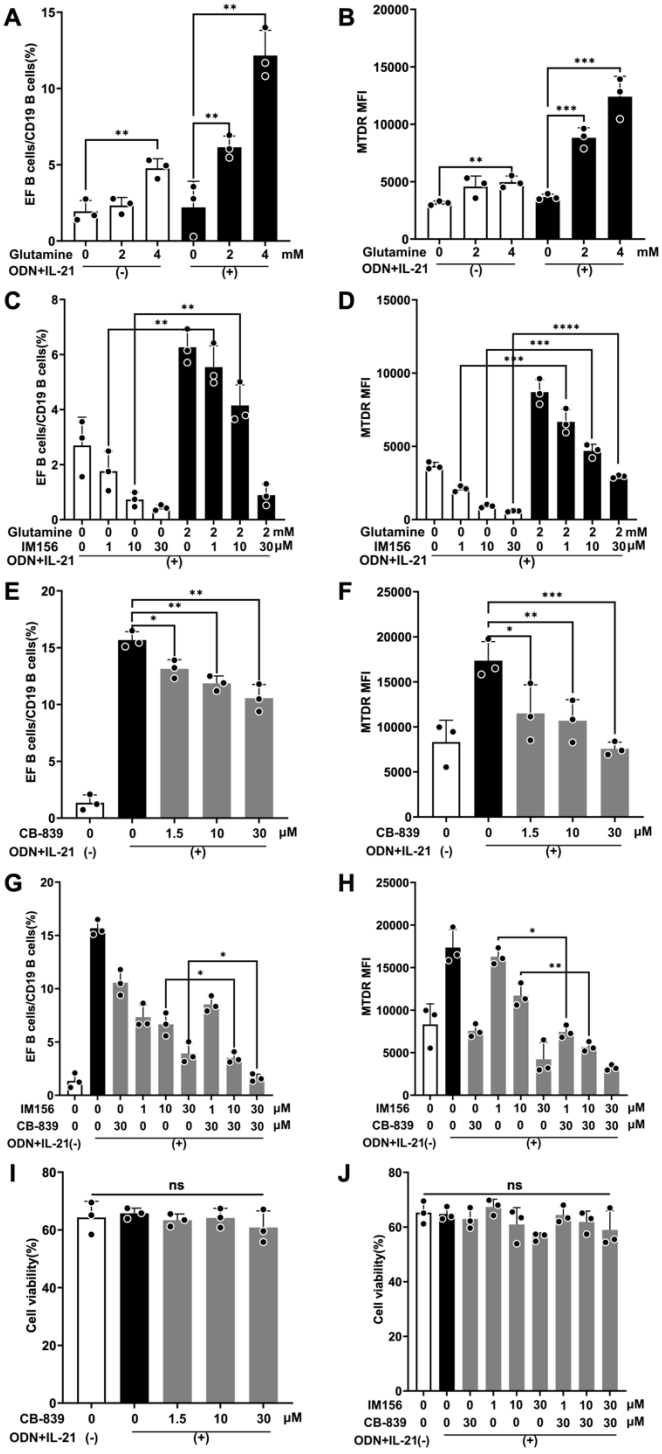

Figure 10. Glutamine metabolism regulates mouse splenic EF B cells *in vitro* differentiation. A concentration of ODN1826 1 μM and IL-21 25 ng/ml was used to induce *in vitro* mouse EF B cell differentiation. **(A)** Percentage ratio of EF B cells/CD19 B cells in splenocytes with glutamine supplement. **(B)** Measurement of MTDR in splenic EF B cells with glutamine supplement. **(C)** Percentage ratio of EF B cells/CD19 B cells in splenocytes treated with IM156. **(D)** Measurement of MTDR in splenic EF B cells treated with IM156. **(E)** Percentage ratio of EF B cells/CD19 B cells in splenocytes treated with CB-839. **(F)** Measurement of MTDR in splenic EF B cells treated with CB-839. **(G)** Percentage ratio of EF B cells/CD19 B cells in splenocytes treated with IM156 and CB-839. **(H)** Measurement of MTDR in splenic EF B cells treated with IM156 and CB-839. **(I)** Percentage of cell viability of mouse splenic cells treated with CB-839. **(J)** Percentage of cell viability of mouse splenic cells treated with IM156 and CB-839. Statistical significance was determined by a two-tailed Student's t-test and one-way ANOVA (*P < 0.05, **P < 0.01, ***P < 0.005, ****P < 0.001; n = 3).

11. Patients with active SLE have upregulated mitochondria ETC metabolism

We examined whole blood RNA-Seq data from a publicly available SLE transcriptome study (27). Our results demonstrated that the ETC pathway was significantly upregulated in patients with active SLE compared with healthy donors (Figure 11A, B, D). In contrast, patients with inactive SLE were similar to healthy donors in terms of metabolic pathway activation (Figure 11C). These findings highlight that the mitochondria ETC metabolism and chemokine activity are important in patients with SLE.

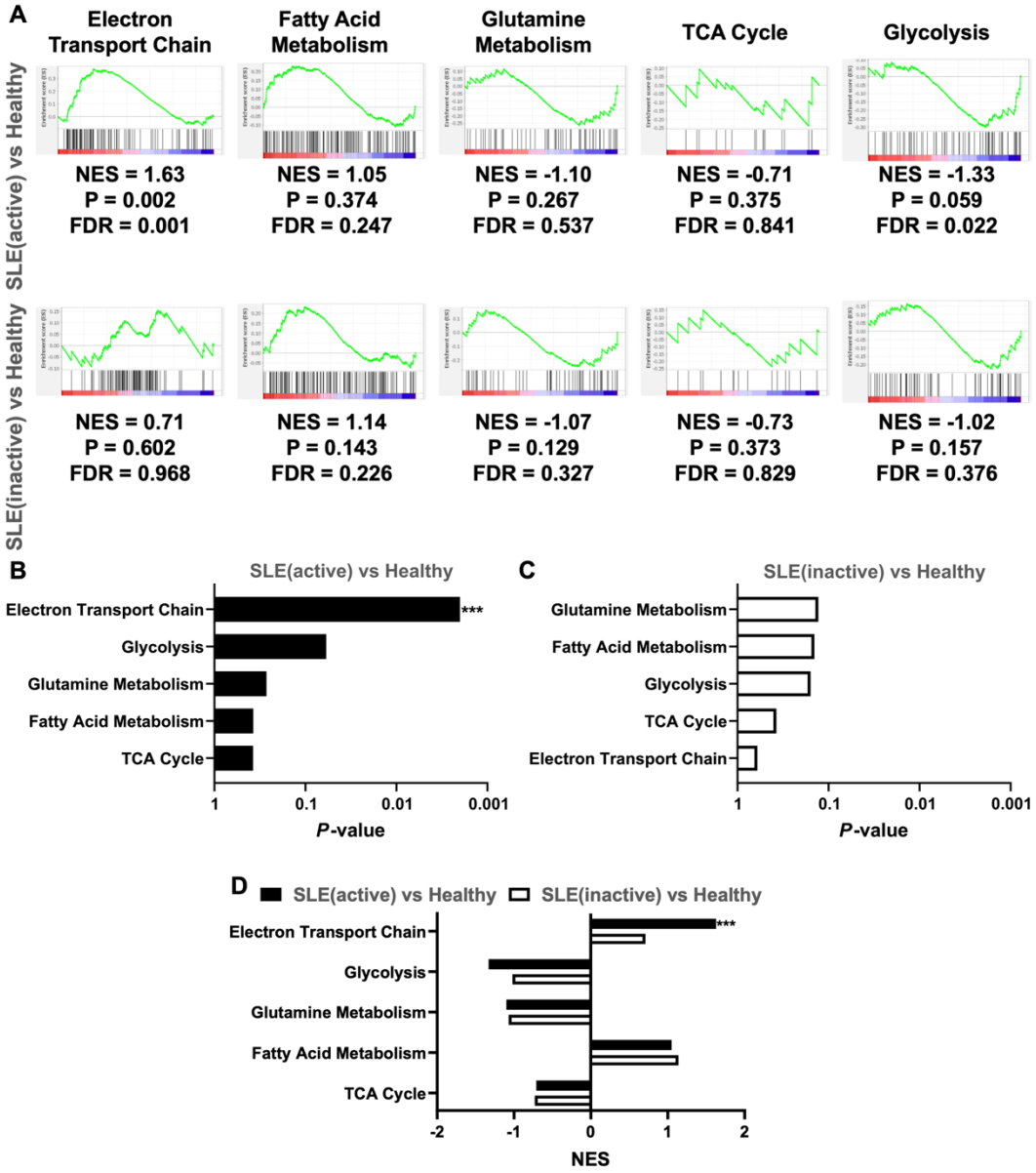

Figure 11. Transcriptome analysis of metabolic pathways in human lupus PBMC. **(A)** GSEA of the electron transport chain, fatty acid metabolism, glutamine metabolism, TCA cycle, and glycolysis. **(B)** P-values of the comparisons between patients with active SLE and healthy donors in GSEA. A logarithmic scale is used on the X-axis. **(C)** P-values

of the comparisons between patients with inactive SLE and healthy donors in GSEA. A logarithmic scale is used on the X-axis. **(D)** Normalized Enrichment Score (NES) for GSEA (***P < 0.005, ****P < 0.001). A false discovery rate (FDR) of <0.25 between any two populations was considered significant.

12. Effect of OXPHOS inhibition on human EF B cells

Using human PBMCs, we investigated the effects of OXPHOS on the generation of EF B cells (CD11c+CD11b+CD19+) (Figure 12). As IM156 inhibits EF B cell generation by suppressing OXPHOS metabolism (Figure 13A, B).

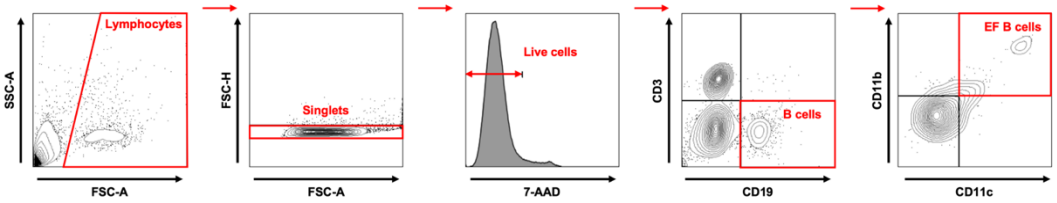

Figure 12. Gating strategy of human extrafollicular (EF) B cells.

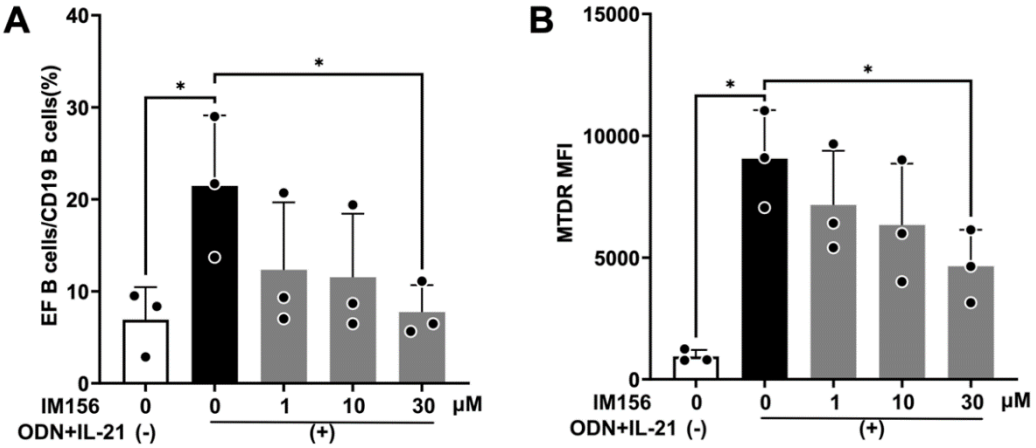

Figure 13. IM156 inhibits human EF B cells in vitro differentiation. A concentration of ODN2006 1 μM and IL-21 25 ng/ml was used to induce in vitro human EF B cell differentiation. **(A)** Percentage ratio of EF B cells/CD19 B cells from PBMCs treated with IM156. **(B)** Measurement of MTDR in EF B cells from PBMCs treated with IM156. Statistical significance was determined by two-tailed Student's t-test. (*P < 0.05; n = 3).

13. Effect of glutamine inhibition on human EF B cells

To confirm the key role of glutamine metabolism in human EF B cells, we also conducted more experiments using PBMCs from patients with lupus. Similar to our results from the *in vitro* mouse assays, the number and mitochondrial activity of EF B cells in human PBMCs increased with higher glutamine concentrations (Figure 14A, B). Of note, IM156 more effectively suppressed the number and mitochondrial activity of human EF B cells in the absence rather than in the presence of glutamate (Figure 14C, D). Moreover, we observed an inverse correlation where the increase in CB-839 concentration led to a decrease in the number and mitochondrial activity in EF B cells (Figure 14E, F). Finally, the combined impact of CB-839 and IM156 exhibited an additive effect in reducing both the number and mitochondrial activity of human EF B cells (Figure 14G, H). In our *in vitro* study, we observed no alterations in human B cell viability at the dosages of IM156 and CB-839 employed (Figure 14I, J). These observations indicate that mitochondrial OXPHOS and glutamine metabolism are critical in human EF B cells.

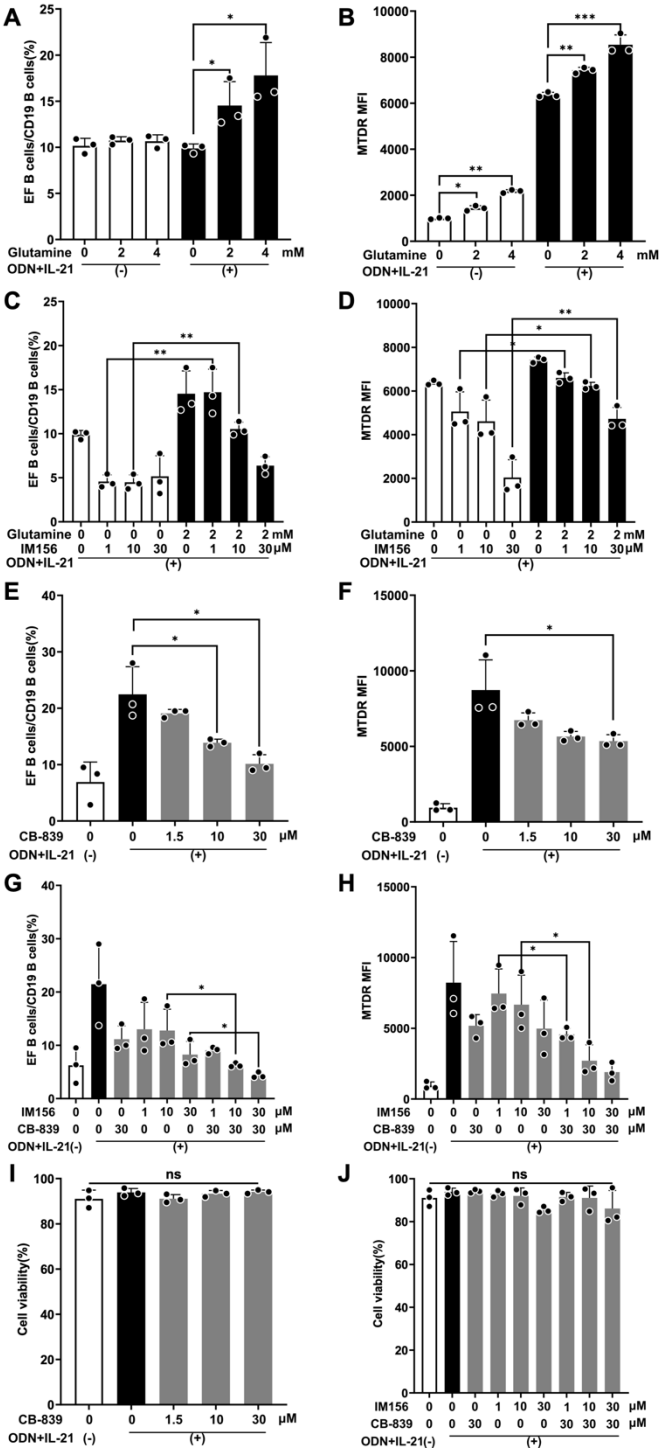

Figure 14. Glutamine metabolism regulates human EF B cells *in vitro* differentiation. A concentration of ODN2006 1 μM and IL-21 25 ng/ml was used to induce *in vitro* human EF B cell differentiation. **(A)** Percentage ratio of EF B cells/CD19 B cells from human PBMCs with glutamine supplement. **(B)** Measurement of MTDR in EF B cells from human PBMCs with glutamine supplement. **(C)** Percentage ratio of EF B cells/CD19 B cells from human PBMCs treated with IM156. **(D)** Measurement of MTDR of EF B cells from human PBMCs treated with IM156. **(E)** Percentage ratio of EF B cells/CD19 B cells from human PBMCs treated with CB-839. **(F)** Measurement of MTDR in EF B cells from human PBMCs treated with CB-839. **(G)** Percentage ratio of EF B cells/CD19 B cells from human PBMCs treated with IM156 and CB-839. **(H)** Measurement of MTDR in EF B cells from human PBMCs treated with IM156 and CB-839. **(I)** Percentage of cell viability of human PBMCs treated with CB-839. **(J)** Percentage of cell viability of human PBMCs treated with IM156 and CB-839. Statistical significance was determined by a two-tailed Student's t-test and one-way ANOVA (*P < 0.05, **P < 0.01, ***P < 0.005, ****P < 0.001; n = 3).

14. Effect of IM156 and CB-839 on Th17 cells

We further investigate the effects of the combination therapy on Th17 cells, another important subset of T cells dependent on glutamine metabolism. Upon exposure to in vitro Th17 lineage-polarizing conditions for 48 hours, naive T cells were differentiated into Th17 cells achieving a differentiation efficiency of up to 50% (Figure 15A). The vast majority of Th17 cells (>97%) demonstrated a notable upregulation of RORγt (Figure 15B). Unlikely EF B cells, in vitro polarized Th17 cells were not suppressed at low dose IM156 (1μM) and the combination therapy did not show a compounding inhibitory effect (Figure 15C). The combination therapy with a high dosage of IM156 (30μM) and CB-839 (30μM) led to a reduction in cell viability of Th17 cells (Figure 15D).

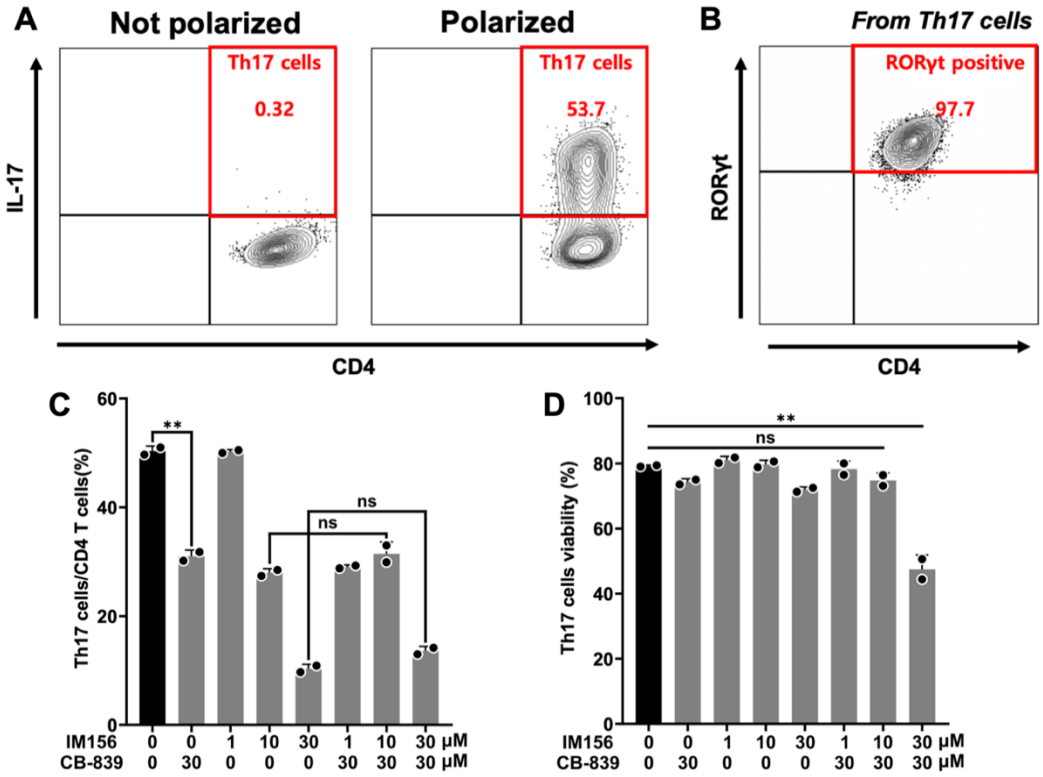

Figure 15. The effect of IM156 and CB-839 on differentiation of splenic Th17 cells. (A) Flow cytometric analysis of Th17 cells (CD4+IL-17+). **(B)** Flow cytometric analysis of RORγt in Th17 cells. **(C)** Percentage ratio of Th17 cells/CD4 cells in splenocytes treated with IM156 and CB-839. **(D)** Cell viability of Th17 cells treated with IM156 and CB-839. (**P < 0.01, ns, not significant.; n = 2)

15. CXCR4 expression in autoreactive EF B cells and plasmablasts

We further investigate the effects of CXCR4 in autoreactive B cells. *In vivo* ODN stimulation increased CXCR4 expression in plasmablasts (Figure 16A). There are also upregulated genes related to chemokine activity, but IM156 is not sufficient to reduce chemokine activity-related genes (Figure 16B). Chemokine genes are significantly upregulated in patients with SLE compared with healthy donors (Figure 16C). Chemotaxis assay revealed that cells of ODN-injected mice have more motility towards SDF-1 (CXCL12) (Figure 16D). Together, our findings indicate that the CXCR4 is important in autoreactive B cells.

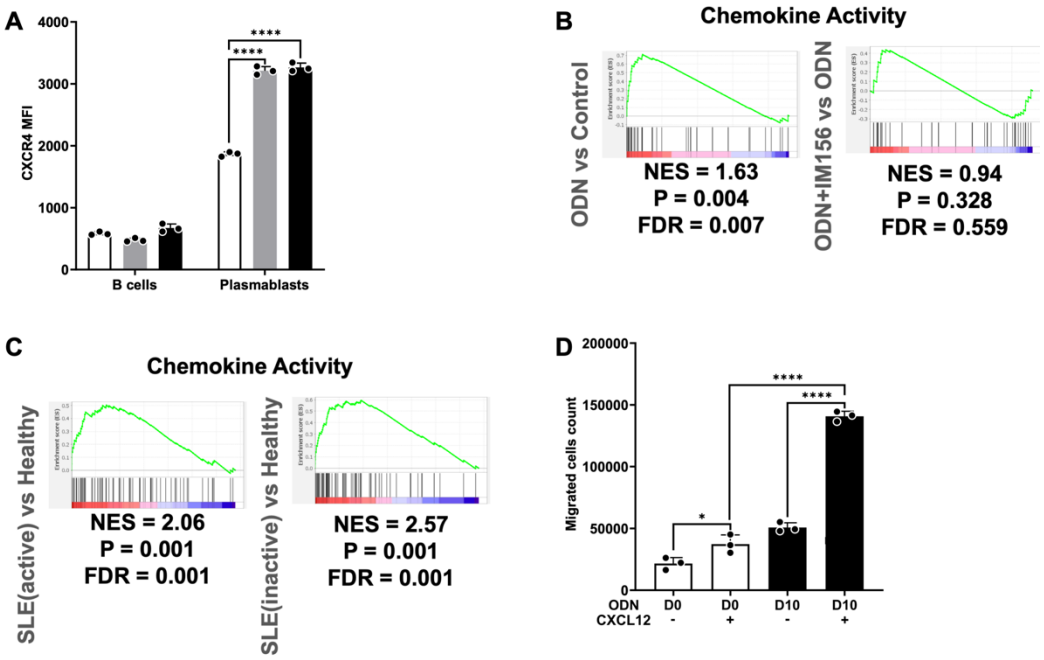

Figure 16. CXCR4 expression in autoreactive B cells. (A) Measurement of CXCR4 expression of B cells and plasmablasts. **(B)** Gene set enrichment analysis (GSEA) of the chemokine activity in mouse B cells. **(C)** Gene set enrichment analysis (GSEA) of the chemokine activity in human PBMCs. **(D)** Chemotaxis assay using splenocyte from ODN injected mice. Statistical significance was determined by a two-tailed Student's t-test (*P < 0.05, ***P < 0.005, ****P < 0.001; n = 3). A false discovery rate (FDR) of <0.25 between any two populations was considered significant; n = 3.

16. AMD3100 suppresses CXCR4 expression of plasmablasts *in vivo*

We evaluated the effect of AMD3100, a CXCR4 inhibitor. As AMD3100 dose increases, EF B cell/CD19 B cells ratio in the mouse spleen (Figure 17A), Plasmablasts/CD19 B cells ratio in the mouse PBMCs (Figure 17B), and Plasmablasts/CD19 B cells ratio in the mouse bone marrows (Figure 17C) decreased. CXCR4 expression was decreased in the plasmablasts by AMD3100 (Figure 17D). Anti-dsDNA IgG titer in mouse and Anti-dsDNA IgG-secreting cells also decreased by AMD3100 (Figure 17E, F) These results shows that CXCR4 critically regulates the migration of auto-immune cells and the function of auto-immune cells. And AMD3100, a CXCR4 inhibitor, effectively represses EF B cells and auto-immune plasmablasts. However, AMD3100 concentrations over 1.5mg/kg, an abnormal increase in the size of the mouse spleen were observed (data not shown).

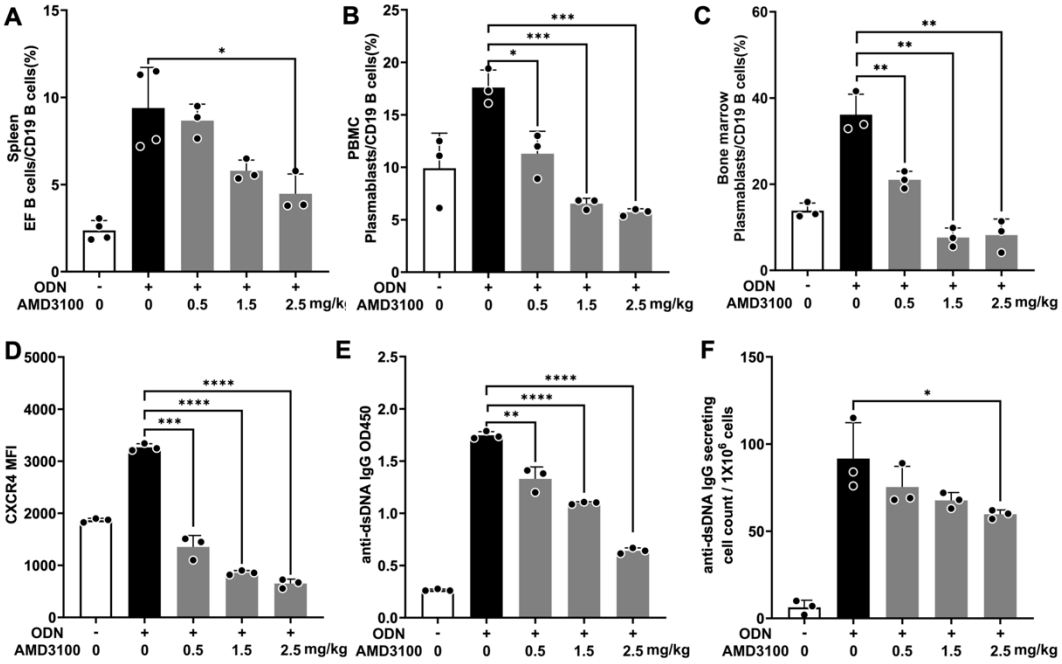

Figure 17. AMD3100 downregulates CXCR4 expression of plasmablasts. (A) Percentage ratio of EF B cells in the mouse spleen with AMD3100. **(B)** Percentage ratio of plasmablasts in the mouse PBMCs with AMD3100. **(C)** Percentage ratio of plasmablasts in the mouse bone marrow with AMD3100. **(D)** Measurement of CXCR4 expression in bone marrow plasmablasts with AMD3100. **(E)** Serum anti-dsDNA IgG levels with AMD3100. **(F)** Counts of anti-dsDNA IgG-secreting cells in the bone marrow with AMD3100. Statistical significance was determined by two-tailed Student's t-test (*P < 0.05, **P < 0.01, ***P < 0.005, ****P < 0.001; n = 3-4).

17. IM156 and AMD3100 downregulates autoimmunity

High concentrations of AMD3100 cause abnormal spleen size increase, and high concentrations of IM156 are toxic. In response, we investigated the effective inhibition of autoimmunity in TLR9-stimulated mice by administering low doses of IM156 and AMD3100. Our findings indicate that there was no observed synergistic effect between IM156 and AMD3100 in EF B cells within the spleen (Figure 18A). However, synergistic effects were evident in the ratio of plasmablasts/CD19 B cells in the blood (Figure 18B) and in the bone marrow (Figure 18C). Notably, the combination of low doses of IM156 and AMD3100 in the bone marrow resulted in the downregulation of plasmablasts to levels comparable to those found in normal mice (Figure 18C). Additionally, synergistic effects were observed in the decrease of MTDR levels in bone marrow plasmablasts (Figure 18D). Conversely, there was no observed synergic effect in the decrease of MTG levels between the treatment with AMD3100 alone and the combined treatment in the bone marrow plasmablasts (Figure 18E). Our results also revealed a synergic effect in the reduction of CXCR4 expression within the bone marrow plasmablasts (Figure 18F). Moreover, the combination of IM156 and AMD3100 led to a synergistic decrease in the levels of anti-dsDNA IgG in mice and a reduction in the population of anti-dsDNA IgG-secreting cells within the bone marrow (Figure 18G, H). Furthermore, our chemotaxis assay demonstrated that IM156 and AMD3100 act synergistically to inhibit migration through CXCR4 (Figure 18I). Overall, these findings demonstrate that the combined treatment of IM156 and AMD3100 significantly contributes to the downregulation of autoimmune plasmablasts.

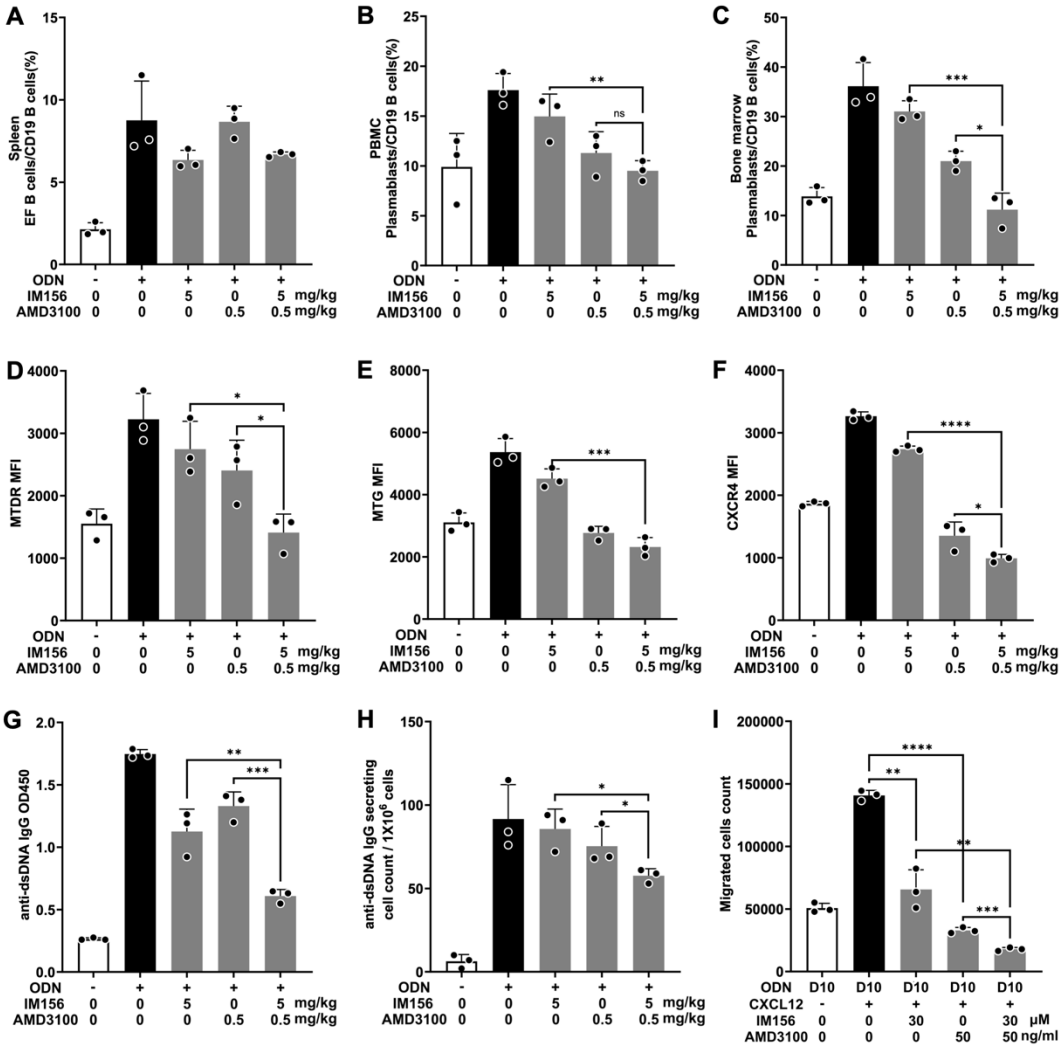

Figure 18. A combination therapy of IM156 and AMD3100 downregulates autoreactive plasmablasts in ODN-injected mice. (A) Percentage ratio of EF B cells in the mouse spleen with IM156 and AMD3100. **(B)** Percentage ratio of plasmablasts in the mouse PBMCs with IM156 and AMD3100. **(C)** Percentage ratio of plasmablasts in the mouse bone marrow with IM156 and AMD3100. **(D)** Measurement of MitoTracker Deep Red (MTDR) in bone marrow plasmablasts with IM156 and AMD3100. **(E)** Measurement of MitoTracker Green (MTG) in bone marrow plasmablasts with IM156 and AMD3100.

(F) Measurement of CXCR4 expression in bone marrow plasmablasts with IM156 and AMD3100. **(G)** Serum anti-dsDNA IgG levels with IM156 and AMD3100. **(H)** Counts of anti-dsDNA IgG-secreting cells in the bone marrow with IM156 and AMD3100. **(I)** Chemotaxis assay of CXCL12 with IM156 and AMD3100. Statistical significance was determined by a two-tailed Student's t-test (*P < 0.05, **P < 0.01, ***P < 0.005, ****P < 0.001; n = 3-4).

IV. DISCUSSION

There has been a surge of published reports recently regarding the altered metabolic pathways of immune cells in patients with SLE (28, 29, 30). CD4+ T cells, in particular, have been shown to enhance both glucose and mitochondrial metabolism in lupus, thereby supporting their chronic activation (29, 31, 32). However, the B cell metabolic programs differ from those of T cells (33). Resting B cells depend more on oxidative phosphorylation than resting T cells and mitochondria perform key functions during various stages of B cell differentiation (10, 22, 33). Nevertheless, the roles of mitochondria in B cells are not well understood in the context of lupus pathogenesis. Our previous study demonstrated that EF B cell development requires mitochondrial OXPHOS metabolism, with an OXPHOS inhibitor improving survival in a mouse model of lupus nephritis (22). Our present work demonstrates that mitochondrial metabolism is also indispensable for the generation of autoreactive plasmablasts.

Plasmablasts are the short-lived effector cells of the early antibody response after acute infection or vaccination (34, 35). Although autoreactive B cell clones are generally removed by immune tolerance mechanisms such as receptor editing or clonal deletion during the B cell differentiation process, autoreactive plasmablasts are increased in autoimmune diseases such as lupus and rheumatoid arthritis (36, 37). Furthermore, disease flares of lupus are marked by a surge in the number of plasmablasts (8, 38). Interestingly, our data highlighted that plasmablasts induced by ODN achieved higher mitochondrial mass and MMP compared to those of plasmablasts from control mice. Transcriptome profiling data showed higher expression of genes related to the electron transport chain in patients with active lupus, while there was no difference in the expression of electron transport chain genes between patients with inactive lupus and healthy donors. Therefore, mitochondrial metabolism inhibitors could be used to suppress lupus disease activity by downregulating autoreactive plasmablast generation.

Metformin, a long-used biguanide for diabetes, was effective when used in combination with 2-deoxy-D-glucose in a murine lupus model. However, animal models have shown

that neither metformin nor 2-deoxy-D-glucose alone is effective (39). The IM156 is a newly synthesized biguanide which has completed a phase I trial in patients with cancer (NCT03272256) and is 60-fold more potent in suppressing mitochondrial OXPHOS metabolism (40). In our previous work, we observed that IM156 downregulated genes related to mitochondrial respiration, cell cycle progression, and plasmablast differentiation in mouse spleen B cells (22). Our current *in vivo* data from bone marrow cells revealed that IM156 suppressed autoreactive plasmablast generation induced by ODN, a TLR9 agonist.

Our current *in vivo* data from bone marrow cells revealed that IM156 suppressed autoreactive plasmablast generation induced by ODN, a TLR9 agonist. However, IM156 alone was not sufficient to revert the number of plasmablasts back to baseline. In addition, our *in vitro* findings suggested that the suppressive effect of IM156 was less potent with the addition of glutamate into the culture media. These findings showcase the importance of glutamine metabolism in plasmablast generation.

During immune cell activation, each cell type has specific metabolic requirements. Effector T cells rely heavily on glycolysis and glutaminolysis, while OXPHOS is a major metabolic pathway for memory T cells and regulatory T cells (41). There is evidence to suggest that glutamine plays a crucial role in B cell activation and differentiation (12, 42). In our study, we observed that glutamine metabolism was important for the generation of autoreactive plasmablasts. *In vivo* mouse data suggested that glutamine metabolism is crucial in antibody-secreting plasmablasts and that the GLS1 inhibitor CB-839 could reduce autoantibody levels. However, the synergistic inhibitory effect of IM156 and CB-839 was not applicable to plasma cell survival. It is possible that the combination strategy of IM156 and CB-839 is more selective to newly generated plasmablasts which have a higher mitochondria metabolism. Our findings are also consistent with those of previous reports. A recent study using a mouse model of lupus nephritis showed that treatment with CB-839 for eight weeks resulted in a reduction in intracellular glutamate levels while there was a significant improvement in proteinuria and renal pathology (43). In another

report, CB-839 treatment on MRL/lpr mice significantly reduced renal IgG deposition (44). Furthermore, glutamine metabolism plays a pivotal role in the differentiation of Th17 cells, which serve as crucial effector cells driving inflammatory processes in lupus nephritis. To comprehensively assess the overall impact of the combination therapy, further evaluation in *in vivo* models is warranted.

Intriguingly, CB-839 administered as a monotherapy does not exhibit inhibitory effects on ODN-induced plasmablasts, whereas IM156 monotherapy does. However, when employed in combination with IM156, CB-839 demonstrates the ability to inhibit plasmablast generation. The additional suppression in plasmablast generation by the GLS1 inhibitor could potentially be attributed to its capacity to inhibit glutamine dependency, triggered by the action of complex I inhibitors. In the present work, the CB-839 dose (15 or 30 mg/kg/day) was several times lower than the dose evaluated in other tumor cell xenograft mouse models (400 mg/kg/day) (45, 46, 47). Our results demonstrated that the simultaneous inhibition of mitochondrial OXPHOS and glutamine metabolism effectively attenuated autoreactive plasmablast differentiation, while low-dose of CB-839 alone was not sufficient to inhibit plasmablast generation. A similar combination strategy using metformin and CB-839 has also been shown to exert a synergistic inhibitory effect in tumor cell xenograft mouse models (15, 16).

Additionally, we investigated the role of AMD3100, initially used for HIV by inhibiting the CXCR4 receptor, in autoimmune diseases (23). It is a slow, reversible, tightly binding inhibitor (48). Several studies have investigated the potential of AMD3100 in various autoimmune conditions such as type I diabetes mellitus (49), DSS-induced colitis (50), collagen-induced arthritis (51), and asthma (52). Another group showed the effect of the co-treatment of AMD3100 and the mitochondria inhibitor metformin on glioblastoma (53). Our investigation is the first study of the co-treatment of AMD3100 and IM156 for autoimmune plasmablast generation.

So far, there are only a small number of studies on the relationship between CXCR4 and mitochondria. Most of them are about how CXCR4 affects mitochondria. The intercellular

connection and transportation of mitochondria in the myeloma tumor microenvironment are supported by the CXCL12/CXCR4 axis (54). The cardiac protective effects induced by CXCR4 overexpression were partly attributed to its regulatory effects on mitochondrial function (55). Another group showed that during lymphocyte migration, mitochondria accumulate specifically at the uropod through shape rearrangements (56). In this study, we presented the initial evidence delineating the impact of mitochondria on CXCR4 expression in lymphocytes.

Our study had certain limitations. First, drugs that modulate mitochondrial function, such as CB-839 or IM156, also promote ROS production. However, we did not address the effects of IM156 or CB-839 on ROS production. Second, although CB-839 and IM156 demonstrated favorable side effect profiles in phase I clinical trials (NCT03272256 and NCT02071862), the systemic effects of the combination strategy also need to be evaluated. Third, we did not assess the impact of combination therapy in murine models of lupus in our current study. Fourth, we did not assess the difference in sensitivity to the inhibition of OXPHOS and glutamine metabolism between healthy controls and lupus patients. Because patients with SLE exhibit evidence of impaired B cell responses to TLR9 stimulation, such investigations hold the potential to identify patients for the application of targeted therapeutic interventions against OXPHOS and glutamine metabolism (57). Fifth, we do not assess the interaction between mitochondria and CXCR4 at the intracellular level. Further studies are needed to clarify the mechanism by which mitochondrial activity affects the expression level of CXCR4.

V. CONCLUSION

Our study underscores the potential of targeting mitochondrial OXPHOS, glutamine metabolism, and the CXCR4-CXCL12 axis to regulate abnormal B cell activation in autoimmune diseases. We propose that a combination therapy involving IM156, CB-839, or AMD3100 could effectively suppress plasmablast differentiation in diseases characterized by abnormal B cell mitochondrial metabolism and CXCR4 expression. This approach holds promise for advancing treatment strategies for such autoimmune conditions.

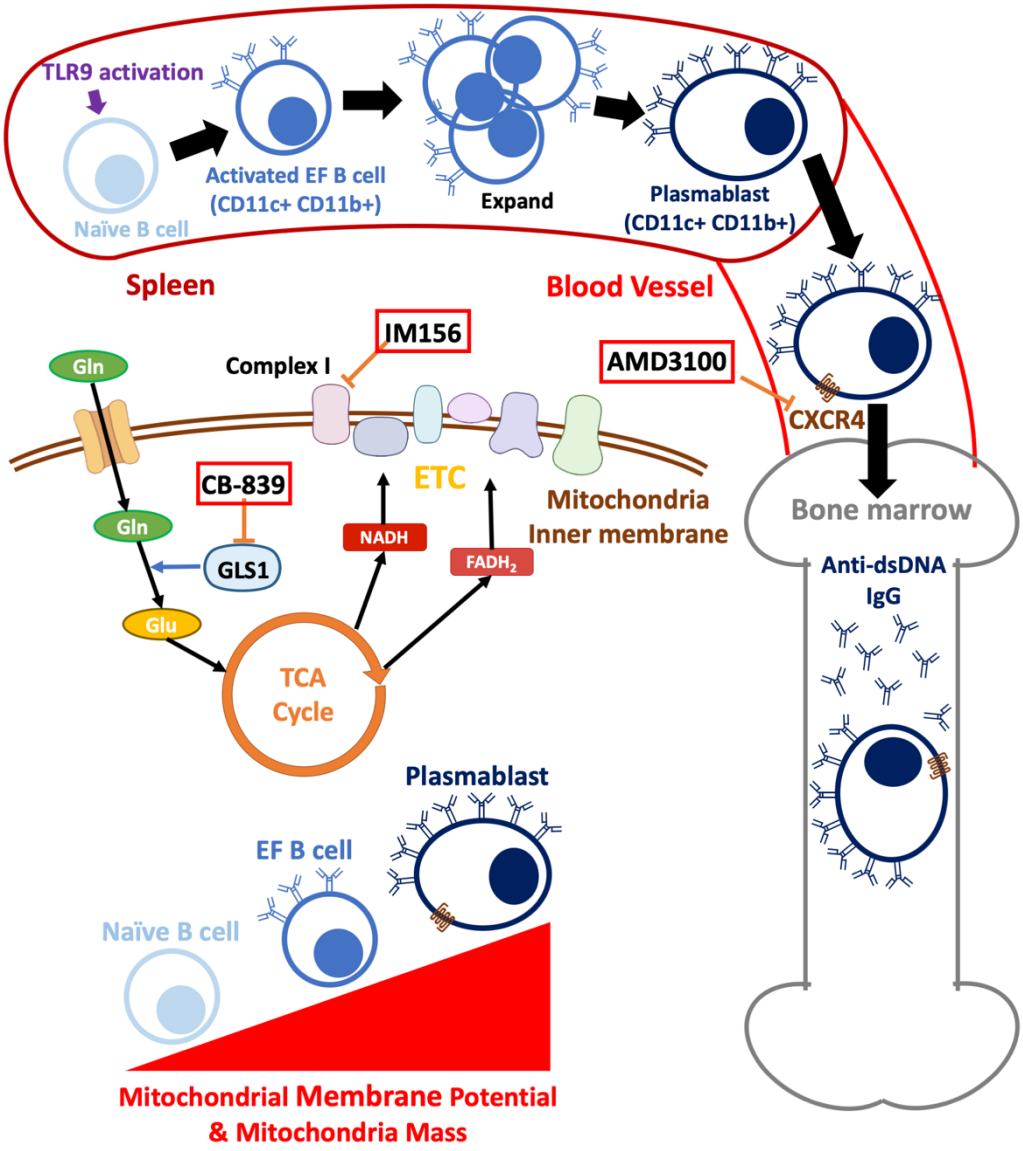

Figure 19. Graphical abstract.

REFERENCES

1. Moulton VR, Suarez-Fueyo A, Meidan E, Li H, Mizui M, Tsokos GC. Pathogenesis of Human Systemic Lupus Erythematosus: A Cellular Perspective. Trends Mol Med. 2017;23(7):615-35.

2. Naradikian MS, Myles A, Beiting DP, Roberts KJ, Dawson L, Herati RS, et al. Cutting Edge: IL-4, IL-21, and IFN-gamma Interact To Govern T-bet and CD11c Expression in TLR-Activated B Cells. J Immunol. 2016;197(4):1023-8.

3. Canny SP, Jackson SW. B Cells in Systemic Lupus Erythematosus: From Disease Mechanisms to Targeted Therapies. Rheum Dis Clin North Am. 2021;47(3):395-413.

4. Elsner RA, Shlomchik MJ. Germinal Center and Extrafollicular B Cell Responses in Vaccination, Immunity, and Autoimmunity. Immunity. 2020;53(6):1136-50.

5. Rubtsova K, Rubtsov AV, Thurman JM, Mennona JM, Kappler JW, Marrack P. B cells expressing the transcription factor T-bet drive lupus-like autoimmunity. J Clin Invest. 2017;127(4):1392-404.

6. Kawasaki T, Kawai T. Toll-like receptor signaling pathways. Front Immunol. 2014;5:461.

7. Lartigue A, Courville P, Auquit I, Francois A, Arnoult C, Tron F, et al. Role of TLR9 in anti-nucleosome and anti-DNA antibody production in lpr mutation-induced murine lupus. J Immunol. 2006;177(2):1349-54.

8. Fillatreau S, Manfroi B, Dorner T. Toll-like receptor signalling in B cells during systemic lupus erythematosus. Nat Rev Rheumatol. 2021;17(2):98-108.

9. Hoppins S. The regulation of mitochondrial dynamics. Curr Opin Cell Biol. 2014;29:46-52.

10. Price MJ, Patterson DG, Scharer CD, Boss JM. Progressive Upregulation of Oxidative Metabolism Facilitates Plasmablast Differentiation to a T-Independent Antigen. Cell Rep. 2018;23(11):3152-9.

11. Sumikawa MH, Iwata S, Zhang M, Miyata H, Ueno M, Todoroki Y, et al. An enhanced mitochondrial function through glutamine metabolism in plasmablast

differentiation in systemic lupus erythematosus. Rheumatology (Oxford). 2022;61(7):3049-59.

12. Crawford J, Cohen HJ. The essential role of L-glutamine in lymphocyte differentiation in vitro. J Cell Physiol. 1985;124(2):275-82.

13. Iwata S, Hajime Sumikawa M, Tanaka Y. B cell activation via immunometabolism in systemic lupus erythematosus. Front Immunol. 2023;14:1155421.

14. Fendt SM, Bell EL, Keibler MA, Davidson SM, Wirth GJ, Fiske B, et al. Metformin decreases glucose oxidation and increases the dependency of prostate cancer cells on reductive glutamine metabolism. Cancer Res. 2013;73(14):4429-38.

15. Ren L, Ruiz-Rodado V, Dowdy T, Huang S, Issaq SH, Beck J, et al. Glutaminase-1 (GLS1) inhibition limits metastatic progression in osteosarcoma. Cancer Metab. 2020;8:4.

16. Qie S, Yoshida A, Parnham S, Oleinik N, Beeson GC, Beeson CC, et al. Targeting glutamine-addiction and overcoming CDK4/6 inhibitor resistance in human esophageal squamous cell carcinoma. Nat Commun. 2019;10(1):1296.

17. Singh AK, Arya RK, Trivedi AK, Sanyal S, Baral R, Dormond O, et al. Chemokine receptor trio: CXCR3, CXCR4 and CXCR7 crosstalk via CXCL11 and CXCL12. Cytokine Growth Factor Rev. 2013;24(1):41-9.

18. Saini V, Marchese A, Majetschak M. CXC chemokine receptor 4 is a cell surface receptor for extracellular ubiquitin. J Biol Chem. 2010;285(20):15566-76.

19. Janssens R, Struyf S, Proost P. The unique structural and functional features of CXCL12. Cell Mol Immunol. 2018;15(4):299-311.

20. Nie Y, Waite J, Brewer F, Sunshine MJ, Littman DR, Zou YR. The role of CXCR4 in maintaining peripheral B cell compartments and humoral immunity. J Exp Med. 2004;200(9):1145-56.

21. Biajoux V, Natt J, Freitas C, Alouche N, Sacquin A, Hemon P, et al. Efficient Plasma Cell Differentiation and Trafficking Require Cxcr4 Desensitization. Cell Rep. 2016;17(1):193-205.

22. Shim JS, Kim EJ, Lee LE, Kim JY, Cho Y, Kim H, et al. The oxidative

phosphorylation inhibitor IM156 suppresses B-cell activation by regulating mitochondrial membrane potential and contributes to the mitigation of systemic lupus erythematosus. Kidney Int. 2023;103(2):343-56.

23. De Clercq E. AMD3100/CXCR4 Inhibitor. Front Immunol. 2015;6:276.

24. Krogmann AO, Lusebrink E, Steinmetz M, Asdonk T, Lahrmann C, Lutjohann D, et al. Proinflammatory Stimulation of Toll-Like Receptor 9 with High Dose CpG ODN 1826 Impairs Endothelial Regeneration and Promotes Atherosclerosis in Mice. PLoS One. 2016;11(1):e0146326.

25. Behrens EM, Canna SW, Slade K, Rao S, Kreiger PA, Paessler M, et al. Repeated TLR9 stimulation results in macrophage activation syndrome-like disease in mice. J Clin Invest. 2011;121(6):2264-77.

26. Clutton G, Mollan K, Hudgens M, Goonetilleke N. A Reproducible, Objective Method Using MitoTracker(R) Fluorescent Dyes to Assess Mitochondrial Mass in T Cells by Flow Cytometry. Cytometry A. 2019;95(4):450-6.

27. Panousis NI, Bertsias GK, Ongen H, Gergianaki I, Tektonidou MG, Trachana M, et al. Combined genetic and transcriptome analysis of patients with SLE: distinct, targetable signatures for susceptibility and severity. Ann Rheum Dis. 2019;78(8):1079-89.

28. Takeshima Y, Iwasaki Y, Fujio K, Yamamoto K. Metabolism as a key regulator in the pathogenesis of systemic lupus erythematosus. Semin Arthritis Rheum. 2019;48(6):1142-5.

29. Teng X, Brown J, Choi SC, Li W, Morel L. Metabolic determinants of lupus pathogenesis. Immunol Rev. 2020;295(1):167-86.

30. Wincup C, Radziszewska A. Abnormal Mitochondrial Physiology in the Pathogenesis of Systemic Lupus Erythematosus. Rheum Dis Clin North Am. 2021;47(3):427-39.

31. Yin Y, Choi SC, Xu Z, Perry DJ, Seay H, Croker BP, et al. Normalization of CD4+ T cell metabolism reverses lupus. Sci Transl Med. 2015;7(274):274ra18.

32. Ma L, Roach T, Morel L. Immunometabolic alterations in lupus: where do they

come from and where do we go from there? Curr Opin Immunol. 2022;78:102245.

33. Boothby M, Rickert RC. Metabolic Regulation of the Immune Humoral Response. Immunity. 2017;46(5):743-55.

34. Fink K. Origin and Function of Circulating Plasmablasts during Acute Viral Infections. Front Immunol. 2012;3:78.

35. Nutt SL, Hodgkin PD, Tarlinton DM, Corcoran LM. The generation of antibody-secreting plasma cells. Nat Rev Immunol. 2015;15(3):160-71.

36. Bonelt P, Wohner M, Minnich M, Tagoh H, Fischer M, Jaritz M, et al. Precocious expression of Blimp1 in B cells causes autoimmune disease with increased self-reactive plasma cells. EMBO J. 2019;38(2).

37. Tan YC, Kongpachith S, Blum LK, Ju CH, Lahey LJ, Lu DR, et al. Barcode-enabled sequencing of plasmablast antibody repertoires in rheumatoid arthritis. Arthritis Rheumatol. 2014;66(10):2706-15.

38. Jacobi AM, Odendahl M, Reiter K, Bruns A, Burmester GR, Radbruch A, et al. Correlation between circulating CD27high plasma cells and disease activity in patients with systemic lupus erythematosus. Arthritis Rheum. 2003;48(5):1332-42.

39. Mack N, Mazzio E, Badisa R, Soliman KFA. Metabolic Response to the Mitochondrial Toxin 1-Methyl-4-phenylpyridinium (MPP+) in LDH-A/B Double-knockout LS174T Colon Cancer Cells. Cancer Genomics Proteomics. 2021;18(3 Suppl):385-405.

40. Willette RN, Mangrolia P, Pondell SM, Lee CYW, Yoo S, Rudoltz MS, et al. Modulation of Oxidative Phosphorylation with IM156 Attenuates Mitochondrial Metabolic Reprogramming and Inhibits Pulmonary Fibrosis. J Pharmacol Exp Ther. 2021;379(3):290-300.

41. Carr EL, Kelman A, Wu GS, Gopaul R, Senkevitch E, Aghvanyan A, et al. Glutamine uptake and metabolism are coordinately regulated by ERK/MAPK during T lymphocyte activation. J Immunol. 2010;185(2):1037-44.

42. Pearce EL, Pearce EJ. Metabolic pathways in immune cell activation and

quiescence. Immunity. 2013;38(4):633-43.

43. Choi SC, Titov AA, Abboud G, Seay HR, Brusko TM, Roopenian DC, et al. Inhibition of glucose metabolism selectively targets autoreactive follicular helper T cells. Nat Commun. 2018;9(1):4369.

44. Zhang X, Wang G, Bi Y, Jiang Z, Wang X. Inhibition of glutaminolysis ameliorates lupus by regulating T and B cell subsets and downregulating the mTOR/P70S6K/4EBP1 and NLRP3/caspase-1/IL-1beta pathways in MRL/lpr mice. Int Immunopharmacol. 2022;112:109133.

45. Gross MI, Demo SD, Dennison JB, Chen L, Chernov-Rogan T, Goyal B, et al. Antitumor activity of the glutaminase inhibitor CB-839 in triple-negative breast cancer. Mol Cancer Ther. 2014;13(4):890-901.

46. Boysen G, Jamshidi-Parsian A, Davis MA, Siegel ER, Simecka CM, Kore RA, et al. Glutaminase inhibitor CB-839 increases radiation sensitivity of lung tumor cells and human lung tumor xenografts in mice. Int J Radiat Biol. 2019;95(4):436-42.

47. Varghese S, Pramanik S, Williams LJ, Hodges HR, Hudgens CW, Fischer GM, et al. The Glutaminase Inhibitor CB-839 (Telaglenastat) Enhances the Antimelanoma Activity of T-Cell-Mediated Immunotherapies. Mol Cancer Ther. 2021;20(3):500-11.

48. Fricker SP. Physiology and pharmacology of plerixafor. Transfus Med Hemother. 2013;40(4):237-45.

49. Leng Q, Nie Y, Zou Y, Chen J. Elevated CXCL12 expression in the bone marrow of NOD mice is associated with altered T cell and stem cell trafficking and diabetes development. BMC Immunol. 2008;9:51.

50. Xia XM, Wang FY, Xu WA, Wang ZK, Liu J, Lu YK, et al. CXCR4 antagonist AMD3100 attenuates colonic damage in mice with experimental colitis. World J Gastroenterol. 2010;16(23):2873-80.

51. De Klerck B, Geboes L, Hatse S, Kelchtermans H, Meyvis Y, Vermeire K, et al. Pro-inflammatory properties of stromal cell-derived factor-1 (CXCL12) in collagen-induced arthritis. Arthritis Res Ther. 2005;7(6):R1208-20.

52. Lukacs NW, Berlin A, Schols D, Skerlj RT, Bridger GJ. AMD3100, a CxCR4 antagonist, attenuates allergic lung inflammation and airway hyperreactivity. Am J Pathol. 2002;160(4):1353-60.

53. Rios A, Hsu SH, Blanco A, Buryanek J, Day AL, McGuire MF, et al. Durable response of glioblastoma to adjuvant therapy consisting of temozolomide and a weekly dose of AMD3100 (plerixafor), a CXCR4 inhibitor, together with lapatinib, metformin and niacinamide. Oncoscience. 2016;3(5-6):156-63.

54. Giallongo C, Dulcamare I, Tibullo D, Del Fabro V, Vicario N, Parrinello N, et al. CXCL12/CXCR4 axis supports mitochondrial trafficking in tumor myeloma microenvironment. Oncogenesis. 2022;11(1):6.

55. Cai WF, Kang K, Huang W, Liang JL, Feng YL, Liu GS, et al. CXCR4 attenuates cardiomyocytes mitochondrial dysfunction to resist ischaemia-reperfusion injury. J Cell Mol Med. 2015;19(8):1825-35.

56. Campello S, Lacalle RA, Bettella M, Manes S, Scorrano L, Viola A. Orchestration of lymphocyte chemotaxis by mitochondrial dynamics. J Exp Med. 2006;203(13):2879-86.

57. Wen L, Zhang B, Wu X, Liu R, Fan H, Han L, et al. Toll-like receptors 7 and 9 regulate the proliferation and differentiation of B cells in systemic lupus erythematosus. Front Immunol. 2023;14:1093208.

ABSTRACT(IN KOREAN)

루푸스에서 자가면역 형질 세포 생성에 대한 미토콘드리아의 역할

<지도교수 송정식>

연세대학교 대학원 의과학과

장성훈

루푸스는 핵항원에 대한 자가항체 생성을 특징으로 하는 자가면역질환이다. 최근 연구에 따르면 형질모세포로 분화할 수 있는 여포외(EF) B 세포가 루푸스에서 중요한 역할을 하는 것으로 나타났다. 우리는 자가반응성 형질모세포 생성에서 미토콘드리아 산화 인산화(OXPHOS), 글루타민 대사 및 CXCR4 발현의 역할을 조사하였다.

생체 내 실험을 위해 쥐에 CpG-oligodeoxyribonucleotides (ODN)을 10일 동안 투여하여 자가반응성 형질모세포의 분화를 유도하였다. B cell의 분화 정도와 미토콘드리아 질량 및 활성 측정은 쥐의 비장, 혈액 및 골수의 세포를 이용하여 유세포 분석으로 분석되었다. 자가반응성 형질모세포의 생성에 대한 평가는 혈청 항-dsDNA 항체와 항-dsDNA 항체 분비 세포를 측정하였다. 시험관내 실험을 위해 루푸스 환자의 말초혈액단핵세포(PBMC)와 쥐의 비장세포를 3일 동안 ODN으로 자극한 후 유세포 분석법으로 EF B 세포의 생성을 확인하였다. OXPHOS 억제제(IM156), 글루타민 대사 억제제(CB-839), CXCR4 억제제(AMD3100)를 사용하였다.

생체 내 ODN 주입은 더 높은 미토콘드리아 활성 및 CXCR4 발현을 갖는 형질모세포로의 B 세포 분화 비율을 증가시켰다. ODN 투여는 항-dsDNA 항체 특이적 형질모세포를 유도했을 뿐만 아니라 항-dsDNA 항체의 수준도 증가시켰다. 시험관 내 ODN 처리는 쥐 비장세포와 인간 PBMC에서 EF B 세포의 생성을 유도하고 미토콘드리아 대사를 증가시켰다. IM156과 CB-839 또는 AMD3100의 조합 전략은 자가반응성 형질모세포를 시너지적으로 억제하였다.

이 연구는 미토콘드리아 대사, 글루타민 대사 및 CXCR4-CXCL12 축이

자가반응성 형질모세포의 발달에 중심적인 역할을 하고, IM156과 CB-839 또는 AMD3100의 조합이 미토콘드리아 OXPHOS, 글루타민 대사 및 CXCR4를 억제하여 자가반응성 형질모세포를 억제한다는 것을 입증하였다. 조합 전략은 비정상적인 B 세포 미토콘드리아 대사 및 CXCR4 발현을 특징으로 하는 자가면역 질환 치료를 위한 유망한 후보가 될 수 있다.

핵심되는 말 : 미토콘드리아, 글루타민, CXCR4, 형질모세포, 루푸스